Abstract

ERICKSON, JODY ANN. Incorporating Carbon Nanotubes into Polypropylene Fibers (Under the direction of BEHNAM POURDEYHIMI)

Carbon nanotubes (CNT) are an exciting new carbon based material discovered in 1991 by Iijima. The size, crystalline structure and conductivity make them an exciting choice for use in a composite fiber. The purpose of this study is to explore the possibilities of melt spinning carbon nanotubes compounded in polypropylene (PP) using conventional spinning equipment.

Carbon Nanotubes, pre-compounded in 30 melt flow rate polypropylene, were purchased from Hyperion Catalysis International at 15% concentration. Let downs from this concentration were spun into fibers using a single screw extruder. However, the resultant fibers exhibited a rough texture and distinct lumps of aggregated carbon nanotubes due to inadequate mixing and dispersion of the concentrated CNT/PP and virgin PP. To address this issue a twin screw extruder was used to compound the polymer into several lower concentrations and a second attempt at spinning yielded greater success. Fibers containing up to 3% CNT were spun as well as some bicomponent fibers. The fibers spun were slightly smoother than those of the initial trial although lumps along the fiber surface are still evident, especially at higher loadings.

Imaging the fibers under optical and scanning electron microscope reveals the extent of the nanotube agglomerate formation and the severe deformation of the fibers. The

aggregates of carbon nanotubes appear in all composite fibers and cause the tensile properties to suffer by acting as stress concentration sites, leading to fiber failure. Conductivity is not achieved even with the highest loading of 3% carbon nanotubes. A uniform distribution of the nanotubes in the polypropylene is believed to be critical to spinning uniform fibers with good mechanical characteristics and to reaching percolation at low loading. CNT aggregation remains a challenge to the processing of these composite fibers.

INCORPORATING CARBON NANOTUBES INTO POLYPROPYLENE FIBERS

By

JODY ERICKSON

A thesis submitted to the Graduate Faculty of

North Carolina State University

in partial fulfillment of the

requirements for the Degree of

Master of Science

DEPARTMENT OF TEXTILE AND APPAREL, TECHNOLOGY AND MANAGEMEMENT

RALEIGH

2 0 0 3

Approved By:

_____	_____
Dr. Behnam Pourdeyhimi (Chair of Advisory Committee)	Dr. Trevor Little
_____	_____
Dr William Oxenham	Dr. Timothy Clapp

Biography

Jody Erickson was born Jody Ann Hutchings, July 30, 1978 in Brockton, Massachusetts. She graduated Loudoun County High School, Leesburg, Virginia in June 1996. After attending the University of Virginia for her freshman and sophomore year, she transferred to North Carolina State University to attend the College of Textiles. In May 2000, Jody graduated Sum Cum Laude with a B.S. in Textile Technology.

After working in the textile industry for a year, Jody returned to the College of Textiles to pursue a Master's degree in Textile Technology. While a graduate student, Jody has enjoyed working as teaching assistant in the short staple spinning and nonwovens laboratories.

After graduating, Jody hopes to work in research and development in the Textile Industry.

Acknowledgements

I would like to extend a special thanks to my advisor, Dr. Pourdeyhimi for his guidance and support of this project. Also special thanks to Dr. Shiffler for his time and energy in traveling and encouragement. Thanks to Dr. Little for providing the funding for materials. Thanks to Mr. Gus Meyer and his technicians, at Fiber Innovations Technology, for the use of their spinning equipment and expertise. Thanks to Ameri Chem for generously donating the using of their compounding equipment. Thanks to the laboratory managers at NCSU and the NCRC staff for making their labs available for advice, testing and storage of materials.

Thanks to my parents, Larry and Geraldine Hutchings, for their love and support. Thanks to my husband, Jeremy, for being the wonderful person he is.

Table of Contents

Page

List of Tables

Page

List of Figures

Page

Chapter One

Introduction

As our society becomes more technologically advanced, the demands placed on a polymer's electrical performance capabilities are continuously growing and becoming increasingly more challenging to satisfy. Technological applications for conductive polymers have evolved to include not only static charge dissipation but reduction of dangerous spark discharge, and electromagnetic interference shielding. Each of these applications requires polymer capable of an increasingly higher level of electrical conduction. Industry is pushing the limits of polymeric materials, seeking a polymer with the conductivity of a metal.

Ideally, this polymer would retain all the same benefits associated with its insulating counterparts: light weight, flexibility, toughness and ease in processing. Its mechanical properties would be consistent with its virgin state or even improved upon. Its aesthetic properties (mainly color) would be unaffected. The polymer would maintain a constant predetermined level of high conduction over its lifetime regardless of environment and its production would be cost efficient.

Currently, there are several methods that can be used to impart conductivity to polymers: doping of intrinsically conductive polymers, incorporation of conductive additives into an insulating polymer matrix and coating of fibers with metals or conductive chemicals. To date, none of these techniques have yielded polymeric fibers able to meet all of the properties proposed in an ideal model. Fortunately, the discovery of a new material,

carbon nanotubes, which can be used as an additive, holds great potential for developing conductive fibers that may come closer to meeting the criteria of the ideal model.

1.2 Purpose

The purpose of this study is to explore the creation of conductive fibers that utilize carbon nanotubes and conventional melt spinning equipment. According to the theory of percolation, the scale and intrinsic high conductivity of carbon nanotubes allow for the formation of a conductive network within an insulating polymer fiber; thus creating a conductive fiber.

There is a technologically driven demand for development of superior conductive fibers and there is concurrently an opportunity to explore a new material that may lead to its' development. Not only could this study lead to the development of a new conductive fiber, but it will also add to the general knowledge of how carbon nanotubes / polymer fiber composites behave.

1.3 Challenges

There are several challenges that face this work. The addition of particles to a polymer melt can cause processing difficulties. Dealing with a new material, these challenges are uncharted. In general, the addition of particles to melts causes them to become more viscous and this can result in the need to alter process parameters. Also how the nanotubes will interact with the melt is of concern; a well dispersed mixed is desired but may be difficult to achieve. Agglomerates may form and interact poorly with filters during spinning. Also the fact that carbon nanotubes conduct heat very well may cause

uneven melt temperature to develop around the nanotubes. Additionally, the percolation threshold, the amount of filler necessary for a lattice of conducting particle to be formed, must be identified in order to achieve conduction. Lastly, drawing the fibers, as necessary for the majority of fiber application, may affect percolation lattices negatively.

Due to material cost and equipment availability, there are several delimitations placed on this study. First, only let downs from polypropylene pre-compounded with 15% by weight of carbon nanotubes will be explored. Second, experimental variables will be limited due to quantity of material available. Third, due to a change in the polypropylene manufacturer's product line, the polypropylene used as the control group contains an added anti-static agent not present in the pre-compounded polypropylene purchased. This addition will confound the results concerning the conductivity of the fibers made.

1.4 Objective

Project objectives are aimed at investigating the interaction between the nanotube and matrix during processing and the properties of the resultant fibers. The primary objective is to investigate the effects of carbon nanotubes on the melt spin processing of polypropylene fibers by spinning composite fibers. The second is to develop bicomponent fibers that allow for maximum conductivity with the least amount of discoloration. Lastly, an investigation of the structural, mechanical and electrical properties of the 100% polypropylene fibers, 100% carbon nanotube / polypropylene composite fibers and polypropylene / composite bicomponent fibers made will be conducted.

Chapter Two

Literature Review

2.1 Electrical Properties of Polymers

The electrical properties of a polymer are characterized by the reaction of the polymer to an electrical field, ε. Where ε is a voltage (V) applied over a given length (L); ε = V/L. As an electric field passes through a polymer, there are four possible reactions: polarization, dielectric relaxation, polymer degradation and conduction[1]. Polarization and relaxation describe the dielectric properties of a polymer, while conduction and polymer degradation describe the bulk conductive properties[1].

The dielectric properties are represented by the dielectric constant (polarization) and the tangent of dielectric loss angle (relaxation). A polymer's dielectric constant, K, is the same as its relative permittivity, ε_R. For polyproplyene, K can range from 2.1-2.6 [2]. It is the polymers ability to store electrical potential energy under the influence of an electric field measured by the ratio of capacitance, C, of a condenser material as a dielectric to its capacitance with a vacuum as a dielectric.

$$C = \varepsilon_0 \frac{A}{l}$$

A = area,

$$C = \varepsilon \frac{A}{l}$$

where l = length between plates

$$\varepsilon_R = \frac{\varepsilon}{\varepsilon_0}$$

$$\varepsilon_0 \equiv 8.85 \cdot 10^{-12} \frac{\text{farad}}{\text{m}}$$

(permittivity of a vacuum)

The electric field causes the formation of dipoles. Different field frequencies result in different types of polarization: electronic, atomic, orientation and interfacial [1]. Polarization causes electron flow to be resisted. Polarization effectively causes a second electric field to form in the opposite direction of the applied resulting in an over all decrease in the electric field. The overall capacitance is increased due to polarization.

The tangent of dielectric loss, tanδ, is related to relaxation phenomenon, the exponential decay of polarization with time once the applied field is removed [1]. There is a time lag in the responsiveness of the molecules in adjusting to the applied field's force. Energy is dissipated in the form of heat when the molecules cannot change conformations at the same rate as an applied field [1]. Alternating currents can accentuate this phenomenon.

$$\tan\delta = \frac{loss\ current}{charging\ current} = \frac{\varepsilon''}{\varepsilon'} \quad [1]$$

The part of the current that is absorbed or lost in the polymer is the imaginary component of the dielectric constant, ε". The measured dielectric constant is ε'.

These reactions are affected by the strength of the applied field. A low intensity field will cause polarization and possibly low levels of conduction in insulators. A higher field may result in increased conduction due to the injection of additional charge carriers, both holes and electrons, from the electrodes [1]. Under even higher electric fields the polymer will begin to decay; the magnitude of the electric field required to cause the localized burning, melting or vaporization of polymer is a measure of the dielectric strength of a polymer [1]. The dielectric strength of a polypropylene film with a

thickness of 10 microns is 300 KV/mm[2]. For a film with a thickness of 6-8nm, the dielectric strength is 1000-1500 KV/mm[2].

An electrical field causes a reorganization of the charges in a polymer if the charges are mobile enough to react in the time frame of the applied field [1]. A direct current will be detected if the charges are mobile enough to diffuse through the specimen and charges can migrate through the electrode/sample interface [1]. No direct current will be detected if the mobility of the charges is spatially limited; this does not mean that polarization will not occur [1]. A charge is spatially limited when it reaches a boundary where it can not be further transported [1]. A boundary may be a polymer molecule or a phase boundary [1].

Figure 2.1 on the following page displays a variety of materials and the conduction values normally associated with them[3]. Note that the usual textile polymers such as nylon or polyester are within the insulating range, $10^{-7}(\Omega^{-1}\ cm^{-1})$ and below. Pure polypropylene has a surface resistance of 10^{15} to 10^{17} Ω [2].

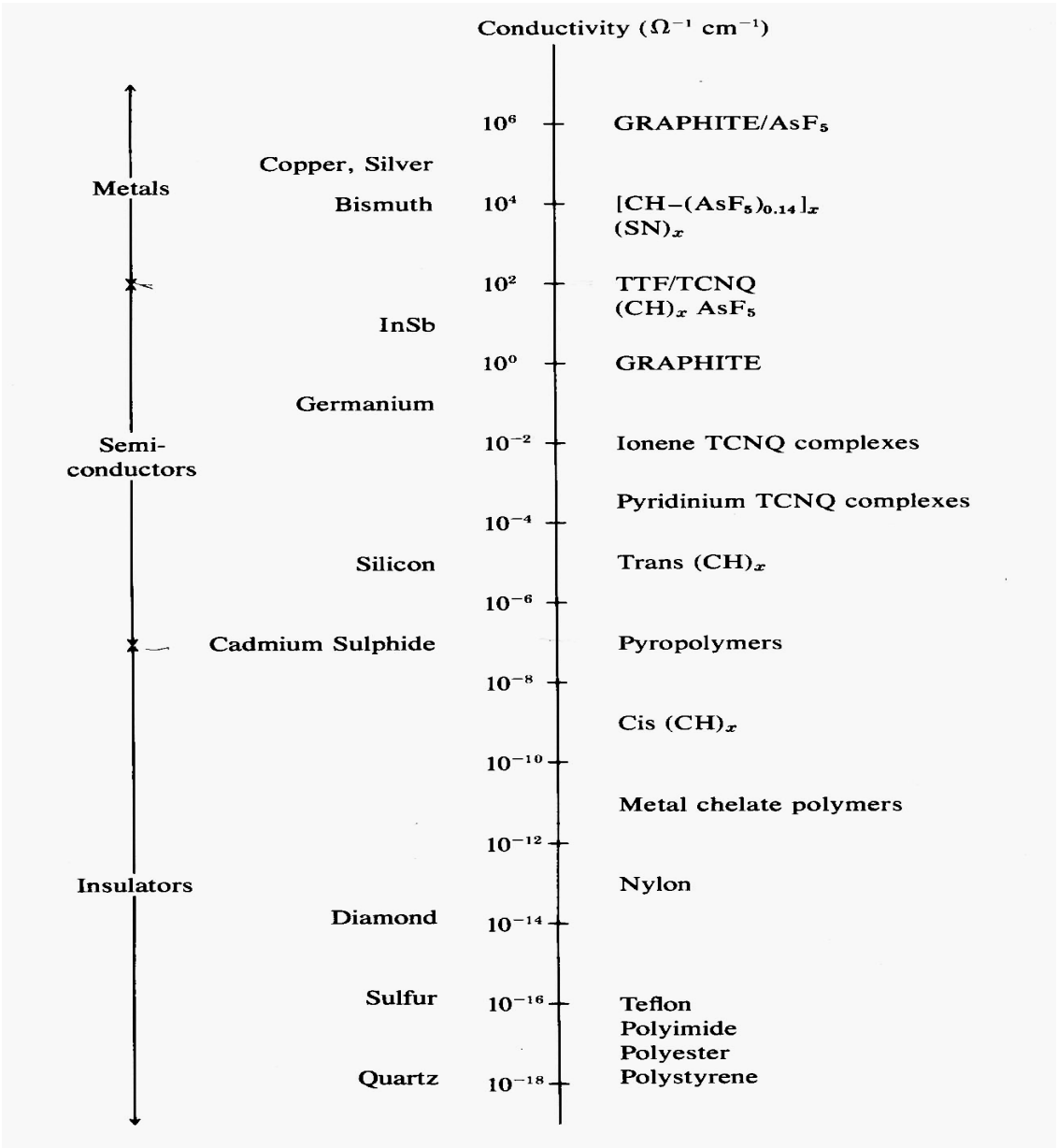

Figure 2.1 Conductivity of Various Materials [3]

2.2 Conductive Polymers

There are several methods that can be used to impart conductivity to polymers: doping of intrinsically conductive polymers, incorporation of conductive additives into an insulating polymer matrix and coating of fibers with metals or conductive chemicals [4]. Each technique has advantages and disadvantages.

Intrinsically conductive polymers suffer from long-term stability issues and problems with processing. Generally ICP are sensitive to oxidation from air and/or acid environments, which will eventually reduce the level of conduction. Also ICP usually exhibit poor thermal stability above 180^{o}C [4]. A major disadvantage of ICPs is that they can only be solution spun; current technology is not available for melt spinning. An advantage of ICPs is that they can reach the same levels of high conductivity that metals can.

Polymer surface conductance is possible through coating metals as well as external and internal additives. Daiwobo Company in Japan has developed a method for coating fibers with a thin (less than 1 micron) layer of copper or nickel. Silver coating of fibers is also done. Antistatic coatings of conducting chemicals may also be applied by dipping, spraying or wiping [4]. A disadvantage of surface coating is the possible effect of reduced conductance due to abrasion and increased toxicity issues from rub off.

Conductive filled polymers have advantages over the previous mentioned techniques because they take advantage of melt spinning polymer processing technology, are cost effective and are less likely to be effected by abrasion. There are two types of additives: liquids and solids. Liquid additives, when incorporated into a polymer matrix, generally work by diffusing to the surface of the fiber (due to a hydrophilic headed molecule) where it interacts with atmospheric oxygen to cause increased surface conductance [4]. Liquid additives fall in three classifications: cationic (alkyl ammonium salts with long polymer chains, glycerol stearate, acid esters and ethoxylated amines), anionic (alkali salts of alkyl sulphonic or phosphonic and carboxylic acids) and non-ionic (ethoxylated alkamines or amides, fatty acid esters, esters or ethers of polyols, glycerol monostearate and ethyloxylate amine) [4]. Non-ionic additives account for over 50% of the market [4]. Solid additives work by forming a network of conductive elements within a matrix polymer.

Filler concentration, shape, size, distribution, and orientation are all important elements that affect percolation. Filler choice is influenced by cost, ability to be dispersed in polymers, affects on mechanical properties of the polymer, required surface structure of the polymer product, wear on production machinery, and the need for high conductivity without the weight of metals [5].

Conductive fillers include carbon in the form of carbon black (spherical shaped particle), nanofibers and more recently describes as nanotubes. Additional popular conductive additives are aluminum, steel, and even metal coated glass fibers. Copper is not used due

to oxidation within the polymer, which negatively affects the physical properties of the polymer [5]. Conventional carbon fiber has an average diameter of 7-10 microns [6]. Nano-carbon fibers have diameters ranging from 50-200nm, hollow inner cores of 30-90nm with lengths that range from 50-100 microns [6]. Multi-walled carbon nanotube (MWNT) diameters range from 2-50 microns while single walled carbon nanotubes (SWNT) are approximately 1nm [6].

Naturally, the benefits of filled polymers do not come without a cost. A common problem is that the additives used at high load levels can cause the polymer's properties to deteriorate. However, fibril shaped additives can significantly reduce the critical volume loading in a manner that is proportional to its linear density [5]. When chunky metal fragments are used, the required volume loading for significant effects is 40-50 percent with weight percentages ranging from 60 to 80% [7]. Carbon is often loaded at 40 % to allow for percolation, but this causes the mechanical properties to degrade to a level where it creates significant problems in producing textile fibers [8]. Longer lengths of the conductive material create longer continuous paths for electrons flow. Thus conductive levels are more quickly reached when fibril structures are used. Additionally, the size and orientation of the particles becomes of paramount concern when fibers are extruded because the area that the particles will take up becomes limited by the diameter of the fiber itself. Not only does the size and shape of nanotubes indicate their potential success as a conductive additive, but nanotubes' additional extraordinary properties make them interesting candidates.

The following table shows the evolution of conductive conjugate fiber structures.

Generation	Cross section	Material and Structure
1 (1950s-)		stainless steel fibres, silver coated organic fibres
2 (1960s-)		organic fibres coated with a carbon black containing polymer
3 (1970s-)		conjugated fibres composed of a carbon black containing polymer and a fibre-forming polymer
4 (1980s-)		conjugated fibres composed of a metallic compound containing polymer and a fibre-forming polymer

Figure 2.2 Evolution of Conductive Conjugate Fibers [9]

2.3 Percolation

Percolation theory is prevalently used to describe conduction and structure in filled polymers so it should be considered in detail. The theory of percolation can be defined succinctly in a mathematical and statistical sense as follows:

> Consider a periodic lattice of sites, each of which is randomly occupied with probability (p) or empty (1-p). Such a lattice contains clusters of neighboring occupied site. As the concentration increases from zero, larger and larger clusters appear. The mean size of the clusters grows and diverges at a well defined threshold, pc. For p > pc there exits an infinite cluster, which connects the two sides of an arbitrarily large sample [10].

Interestingly, percolation theory has its roots in polymer chemistry development during World War II [10]. It was used to describe the gelation phenomenon seen while creating

cross-linked polymers. In this case however, all the polymer chains are already present in the system and it is the formation of chemical bonds that create the lattice, not whether a site is occupied or not. Thus, a modified version of percolation theory is needed to describe this system. It states that all sites are occupied and the bonds formed between neighbors are random with probability (p) of being connected and probability (1 - p) of not being connected [10]. Additionally in this modified model, a cluster is a group of neighboring sites connected by bonds [10].

P. Flory and W. Stockmayer, using a Bethe lattice and the assumptions of no cyclic links or minimum distances for certain parts of the polymers, defined the percolation threshold (pc) equivalent to 1/(f-1) where f is the functionality of the polymer[10]. At the percolation threshold, an infinitely large cluster is formed. As a result, there is a distinct phase transition observed where there is a qualitative change in the system. The term percolation and its application to a regular lattice occurred in 1957 [10].

Computer simulations or mathematics are used to find the pc values. Table 2.1 gives the pc values for some common lattice structures for both bond and site percolation as earlier discussed [10].

Table 2.1**:** Percolation threshold values for common lattice structures [10]

Lattice	Site	Bond
Honey Comb	0.696	0.653
Square	0.593	0.500
Triangular	0.500	0.347
Simple Cubic	0.312	0.249
Body Centered Cubic	0.245	0.178
Face Centered Cubic	0.198	0.119
4-D Hypercubic lattice	0.197	0.160

For each site or potential bond, a random number between zero and one is generated [10]. If this random number is greater than p then it is occupied or a bond is formed, otherwise it is not [10].

For systems with $p < pc$, an average cluster size can be found [10]. The mean cluster size diverges towards infinity as the percolation threshold is approached and an infinite network established [10]. The typical cluster radius, ξ, is defined as the root mean square average distance between two randomly selected occupied sites within the same cluster [10]. The cluster size S can also be defined [10]. Additionally one can investigate the fraction of sites included in the infinite cluster in an infinite system, $P\infty$ [10]. When p is very near pc, power laws defined by critical exponent can be used to describe to how $P\infty$, ξ and S behave [10].

$P\infty$ is proportional to $(p-pc)^{\beta}$, where $p > pc$

S is proportional to $(pc-p)^{-\Upsilon}$, where $p < pc$

ξ is proportional to $(pc-p)^{-\upsilon}$ where $p < pc$

Table 2.2: Values for percolation exponents for two, three, and high level dimensions[10]

Exponent	d = 2	d = 3	$D \rightarrow \infty$
β	5/36	0.42	1
Υ	43/18	1.80	1
υ	4/3	0.88	½

Table 2.2 displays the common values for the percolation exponents for the various dimensions given as d. The actual lattice shape has no bearing on these predictions; only its dimension is important [10].

A key element related to percolation is fractal geometry developed by Mendelbrot [11]. Fractal geometry theory allows for a quantitative description of the disordered aggregates through a fractal dimension [11]. Fractal dimensions can be used to characterize cluster aggregates. A fractal can be defined as an object in which its mass increases proportionally to its $(\text{length})^{\wedge D}$ where D is its fractal dimension [10]. For an object to be a fractal it must be self-similar [10]. Self-similar means that it is scale invariant (i.e.

zooming in or out yields the same appearance). Figure 2.3 is an example of a self-similar object known as a Sierpinski Triangle.

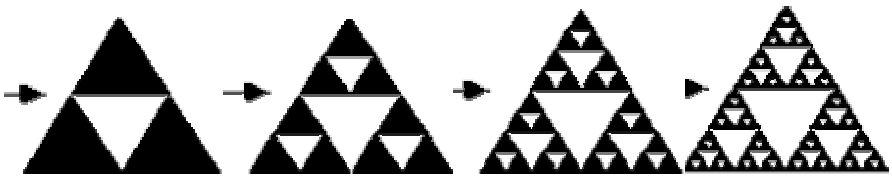

(http://math.rice.edu/~lanius/fractals/)

Figure 2.3: Sierpinski Triangle

If a lattice of length, L, and dimensions, d, such that L^d gives its size is considered then above pc, ξ is comparatively small to L [10]. Thus, the largest cluster fills the sample uniformly with a density equal to P∞ [10]. The number of sites included in the cluster can now be given by the equation [10]:

$$M(L) = L^d P\infty \ \propto L^d (p - pc)^{\beta} \propto L^d \xi^{-\frac{\beta}{\nu}}$$

Due to self-similar attributes, this equation can now be reduced using fractal dimensionality to the equation [10]:

$$M(L) = L^D$$

Table 2.3**:** Other exponent values for percolation [10]

Exponent	d = 2	d = 3	$d \to \infty$
D (p=pc)	91/48	2.52	4
D (p<pc)	1.56	2	4
D (p>pc)	2	3	4

Plotting the log of the number of sites, M(L) in the largest cluster, verses the log of the lattice size, L^d at its percolation threshold, yields a straight line [10]. The slope of the line is fractal dimension, D, for the system [10]. Table 2.3 presents values associated with D for a given comparison of the probability to the percolation threshold value and dimension of the lattice [10].

For metal filled polymer films, the aggregate's length, L, is replaced by the radius of gyration, R, which more adequately describes the structures [11]. The equation giving the number of particles in an aggregate is now given by [11]:

$$N \approx R^D$$

where D is the fractal dimension.

How aggregates are formed is explained through three disputing colloidal theories. These main theories are diffusion-limited aggregation (DLA), reaction-limited aggregation (RLA), and the ballistic theory [11]. In the DLA model, diffusing particles collide with each other to form aggregates or collide with already existing aggregates to create new aggregates [11]. When the particles hit one another, a rigid instantaneous

bond is made [11]. In the RLA model, diffusing particles collide with each other to form aggregates or with already existing aggregates as in the DLA model, but the probability of a bond being formed is unlikely [11]. Ballistic models assume that the particles move in linear trajectories in space [11]. Table 2.4 displays some experimental results [11].

Table 2.4: Experimental results [11]

Diffusion Limited Aggregates			**Reaction Limited Aggregates**		**Ballistic**
	D = 2	d = 3	d = 2	d = 3	d = 3
Irreversible Particle/Cluster Collision	D = 1.7	D = 2.5			
Cluster/Cluster Collision	D = 1.48	D = 1.78	D = 1.53	D = 1.98	D = 1.91

Numerical analysis of optical or electron microscopy images is the most used method for experimentally determining fractal dimensions [11]. Additionally, small angle neutron, X-ray or light scattering methods can be used [11].

After reviewing percolation theory and understanding how fractal geometry and colloidal dispersion affect cluster formation, it is fitting to now apply percolation to conduction. All sites or bonds occupied are considered to be conductive while unoccupied sites or non-bonded elements are considered insulators [10]. Circuit theory suggests that electric currents can only pass between conductive neighbors [10]. It is assumed that the

conductivity, Σ, is zero when p<pc, and nonzero when p>pc [10]. The equation used to describe conductivity is [10]:

$$\sum \propto (p - pc)^{\mu}$$

where μ is given in table 2.5.

Table 2.5 Values of the exponent in the conductivity equation for a given dimensionality [10]

Exponent	d = 2	d = 3	$d \to \infty$
μ	1.3	2.0	3

Numerical simulation using the Monte Carlo method can give values for pc in an unordered system [11]. This method involves multiple simulation steps, where at each step a probabilistic approach is used for accepting or rejecting the next step in the simulation until the chain converges [11]. In lattice models, conductivity can be considered through analysis by using either points or bonds [11]. In the points model, conductive bonds are the lattice points themselves, and in the bond case there are bonds between the lattice points which are conductive [11]. In either case, clusters are formed from connecting conducting points of nearest neighbors[11]. When the system is made up of bonded elements the equation is,

$$Z \bullet pc = \frac{d}{(d-1)}$$

where Z is the number of nearest neighbors and d is the spatial dimension [11]. When the system is considered to be point orientated, the percolation threshold is represented as [11]:

$$pc = \frac{\theta_C}{\gamma}$$

The variable ϒ is a coefficient dependant on the lattice structure or "packing density" [11]. For three dimensions θ_C = 0.15 +/- 0.02 and for two dimension θ_C = 0.45 +/- 0.03 [11].

Understanding the interactions necessary to create conductive metal filled polymer composites can be quite complex. The filler concentration must be that of the percolation threshold for an infinite network to be formed and conduction to occur. Conduction is expected to occur over the lattice network formed by the filler, and not by way of the matrix due to its insulator nature. The properties of the matrix, filler, filler concentration, and how the composite was made have huge implications on conduction. Additionally, there are other influences, including polymer interlayer thickness between conducting elements, physiochemical properties, temperature, and strength of external fields, which add to electron tunneling or ionic conduction [11].

Interaction energies for the polymer matrix and conductive elements are very important in determining the polymer interlayer thickness. If the filler-filler and filler-matrix interaction energies are similar, then a random distribution of particle sizes with in the matrix may be able to occur [11]. This means that the theoretical percolation

concentration and the experimental results will fit more closely [11]. However, if the filler-matrix interaction energies are stronger than the filler-filler energies, then the filler particles will want to bond with the matrix and create insulating layers around them [11]. On the other hand, if the filler-filler interaction energies are greater, then the fillers will want to interact with one another and create the lattice network more efficiently [11]. The interlayer thickness can vary from 10-100 angstroms [11].

The polymer interlayer thickness causes a lot of havoc in the predicting conductance. Conductivity is determined by resistance of direct contact or by the properties of the inter-particle layer where the tunnel effect allows electrons to pass through the thin layers [12]. The maximum expected conduction of a conductive composite with random fiber orientation is given as follows:

$$\sigma_{max} = \frac{2}{3} \Pi \varphi \sigma_f \quad \text{where}$$

φ is the volume fraction and σ_f is the conductivity of the fiber additive.

This layer can act to separate the conductive particles, potentially inhibiting conductance if the particles are too thick. When the insulating layer limits particle contact such that the contact area is less than that of its cross section transient, resistance is also developed [11]. This contact resistance causes a region of smearing to appear [11]. The region of smearing represents the area of critical transition from one state to another [11]. It affects the percolation threshold, pc, and it is the cause of discrepancies between theoretical pc values and experimental pc values [11]. Figure 2.4 is a graph of the log of conductance, σ, verses the particle concentration, p [11].

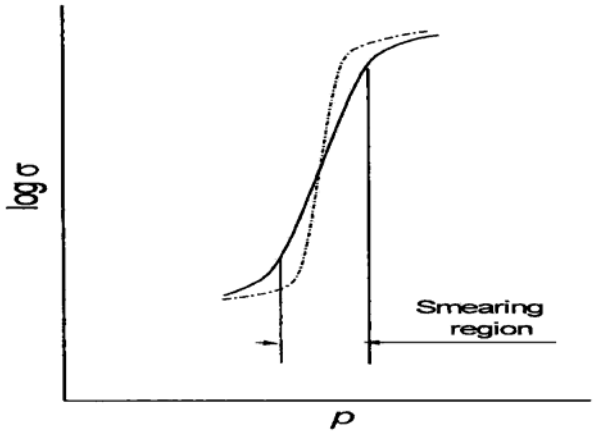

Figure 2.4: Graph of the log of conductance versus particle concentration [11]

Note there is a sudden, large increase in conductivity due to attaining an optimum level of additive. Percolation has to be reached for the polymer to become highly conductive.

2.4 Carbon Nanotubes

The discovery of carbon nanotubes stemmed from research carried out in the mid 1980s at Rice University[12]. At that time, Smalley and his co-workers developed the chemistry of fullerene structures, which resulted in the synthesis of nanotubes. Nanotubes were first reported by Japanese electron microscropist, Iijima, in 1991[14]. Iijima discovered multi-walled nanotubes while examining the byproducts of an experiment involving direct current arc discharge between carbon electrodes in a helium environment at 3000°C[14]. Since their discovery, nanotubes have been catapulted into the forefront of scientific investigations. The mostly defect free structures with high intrinsic strength, due to sp^2 C-C bonds, are predicted to have the highest modulus and strength of any

known material[15]. In addition to these impressive mechanical properties, nanotubes display remarkable electrical and thermal properties.

Carbon nanotubes are needle-shaped, single crystals[15]. Their properties depend on the atomic arrangement, chirality, diameter, and length of the tube and the overall morphology[13]. Nanotubes exist in one of two structural forms, single walled (SWNT) or multi-walled (MWNT). SWNTs are best described as a 2-D graphene sheet (a hexagonal array of carbon atoms) rolled into a tube with pentagonal rings as end caps[13,14]. SWNTs have aspect ratios of 1000 or more and an approximate diameter of 1nm or 10 angstroms[14]. Similarly, MWNT can be described as multiple layers of concentric graphene cyclinders also with pentagonal ring end caps[14]. Nanotubes, depending on the method of synthesis, are often formed in entangled ropes with 10–100 nanotubes per bundle[14]. The surface of the tube is smooth and relatively defect free. However, stresses can induce Stone Wales transformations, resulting in the formation of heptagons and concave areas of deformation on the tubes[13].

Currently, nanotubes can be produced by a number of methods: direct-current arc discharge, laser ablation, thermal and plasma enhanced chemical vapor deposition (CVD) and self-assembly of single crystals of SWNT[14]. The method of production affects the level of purity of the sample and whether SWNTs or MWNTs are formed. Impurities exist as catalysis particles, amorphous carbon and non-tubular fullerenes[13].

Studying individual CNTs is a difficult proposition. Existing challenges lie in the scale of these structures. There is a lack of tools for direct measurements[13]. Uncertainties are introduced to measurements by indirect methods and there are limitations on specimen size[13]. Also, test specimen preparation techniques have not been perfected so that there is not precise and accurate control in nanotube production[13]. Thus, the mechanical and electrical properties show range of values.

The tensile modulus of CNTs is said to be in the range of 270GPa to 1TPa and the tensile strength to be in the range of 11-200 GPa which is stronger than graphite, Kevlar, and 100 times stronger than steel [14]. Yu et al., testing tensile loading using AFM, found that MWNT failed in a telescoping mechanism [13]. They found the outer layer to range between 1 and 63 GPa, and the elastic modulus to range between 270 and 950 GPa [13]. Their tests on SWNTs revealed a tensile strength of 13-52 GPa and an average elastic modulus between 320 and 1470 GPa [13]. Walters et al. reported a yield strength of 45.7 GPa, calculated using strain measured with AFM and an assumed valued of 1.25TPa elastic modulus [13]. Wong and associates used AFM to measure elastic modulus of 1.26TPa and bending strength of 14.2 +/- 0.8 GPa on MWNTs. Yakobson et al. noted that nanotubes are extremely resilient to strain without brittleness or plasticity due to Stone Wales transformations during plastic deformation [13]. They theorize ductile fracture in armchair nanotubes. After Stone Wales defects occur, brittle cleavage or ductile flow results depending on tube symmetry, applied tension, and temperature [13]. High strain at low temperature induces a brittle response. At low strain at high temperatures and a tube diameter less than 1.1nm results in ductile responses; however,

large diameter tubes respond in a moderate or completely brittle manner[15]. Bending is reversible up to 110 degrees[13]. Vigolo et al. successfully knotted SWNT fibers without breakage, showing their incredible plastic behavior[14]. Tersoff and Ruoff, show that tubes with diameters less than 1nm are rigid, but those with diameters of 2.5nm or greater undergo a radial deformation due to Van der Waal forces [14].

The conductive properties of nanotubes are also heavily dependent on their structure, which is characterized by the chiral angle and diameter of the tube [14]. In fact, the conducting properties range from metallic to semi-conducting (electron band gap of 0.5eV) [14]. The band gap decreases with increasing diameter [14].

$$E\ gap = \frac{2\gamma_0 a_{c-c}}{d}$$

where γ_0 is the carbon bonded to carbon tight binding overlap energy of 2.45eV, and the a_{c-c} is the nearest neighbor carbon to carbon distance of approximately 1.42 angstroms.

Some nanotubes have the capacity to carry electric current that is 1000 time greater than copper wires[13].

The chiral angle (θ) is measured as the angle between the chiral vector (C_h), with respect to the zig-zag direction and the unit vectors a1 and a2[14]. The chiral vector is related to the unit vectors by Ch = na1 +ma2, where n and m are lattice translation indices[14]. When θ = 0 and (n,0), the nanotube has semi-metallic conduction and is "armchair"

conformation[14]. When θ = 30 (n,n), the nanotube has metallic conduction and is "zig-zag" conformation[14]. All other angles are characterized by the lattice translation indices. When n-m = 3p and p is an integer, the expected conduction is metallic[14]. When p is not an integer the conduction expected is semi-metallic with an energy band gap around 0.5eV[14]. Carbon nanotubes are thermally stable in a vacuum at temperatures up to 2800 C[13]. Their thermal conductivity is twice that of a diamond[13].

It is easy to see why there is such fascination with this material since it holds so much promise for unique applications. However, trying to capture these properties on a macroscopic scale presents several challenges and currently many resources are being applied to determine how to best harness the capabilities of carbon nanotubes. While incorporating nanotubes into composite fiber structures offers one solution, other methods such as using solution, electrophoretic, or silk-like spinning techniques to create fibers solely of carbon nanotubes are also being explored. These techniques are still in their infancy stages in the laboratory. Only composite technology can offer the possibility of wide scale production today because of its use of current, available technology and the fact that it generally requires only small amounts of nanotubes. U.S. Patent 6,299,812B1 describes a general method for the process of melt spinning and melt blowing carbon nanotube/polymer composites [16]. Carbon nanotubes are expensive due to limited supplies.

Challenges to making successful CNT/polymer composites arise from the smooth and relatively inactive chemical structure of the carbon nanotubes. Low adhesion and matrix wetting mean that composites could potentially suffer from poor dispersion and fiber pull-out. Composite reinforcement from nanotubes may result in increased toughness due to energy absorption from fiber/matrix de-bonding, but not necessarily increased strength, which is derived from a transfer of energy load from the matrix to the fibers.

The number one challenge to incorporating CNTs as fillers for polymers is dispersion. In order for fibers with good mechanical and conductive properties to be formed, good dispersion within the polymer matrix is required. Van der Waals forces, which cause the CNTs to clump together and form aggregates, must be overcome. The use of solvents and mechanical action (sonication) are one approach to solving this problem. Solubility is another problem since nanotubes will not disperse in organic solvents. Several studies have been preformed where investigators have experimented with different methods of combining nanotubes and polymer matrices.

Prior Work

Carole A. Cooper et al. successfully developed a technique of dry powder mixing to form PMMA and nanotube composites[17]. MWNTs and SWNTs were dispersed in a small amount of ethanol using an ultrasonic processor (Vibracell VCX 600) at 10% amplitude for 90s. The PMMA polymer particles were also sonicated in ethanol at the same amplitude and time. The ethanol, PMMA, and CNTs were then combined together and further sonicated at 50% amplitude for 90s. Confirmed by SEM micrographs, this action

caused the CNTs to coat the surface of PMMA particles. Coating the particles prior to mechanical mixing is thought to prevent particle clustering. The ethanol was vacuum dried from the mix at 50 C for 1-2 hours. Next, the coated PMMA particles were mechanically mixed using a Molinex Attitor. This was followed by kneading at 170 C with a laboratory size twin screw compounder (Brabender Plasti-Corder) at 30-50 rpm for 10-30 minutes to form a uniform viscous mass. Finally, a Brabender DSK 25 single-screw extruder with 25mm screw diameter, L/D ratio of 22, melt temperature of 232 C and 16 bar of pressure in the first stage was used to extrude a composite from the slit die. Once extruded, the composite was water quenched. Image analysis from TEM micrographs and Knoop hardness testing confirmed that the orientation distribution was highly orientated in the flow direction of extrusion.

R. Haggenmueller et al. developed a method for preparing nanotubes for melt spinning [18]. The investigation combined nanotubes of different levels of purity that had been pre-sonicated in DMF, with a 10% solution of PMMA dissolved in DMF, which were then sonicated together for an additional 3 hours. The combined solutions were then prepared in two ways: directly solution cast and dried as films, or directly solution cast, dried and then broken into pieces that were melt compressed several times over. The melt compressed composites resulted in highly dispersed films and were further spun into fibers and drawn at different ratios. While the publication reports improved mechanical properties of the fibers, they report the fibers' surfaces to be irregular with the additional of the SWNTs. Using electrical conductivity as a test, the experiment showed that as the draw ration increased, the weight fraction for needed percolation also increased.

Kumar et al. conducted a study in which they prepared and tested polypropylene and carbon nano fibers [6]. The fibers, 55 microns in diameter, were made by small scale conventional techniques which included mixing the PP(95g) with the carbon nanofibers (5g) in a Haake rheocord 90 twin screw extruder (TW100), and then extruding the fibers at 20rpm through the four temperature zones, 150, 220, 220, and 240 degrees Celsius. The material was quenched in a room temperature bath, palletized and dried under a vacuum of 80 degrees Celsius. It was shown that with a 5% loading there was no significant affect in the tensile modulus of the composite fibers. However, there was significant decrease in tensile modulus, 7.1 +/- 0.9 GPa to 4.6 +/- 0.8 GPa. The compressive strength increased from 25+/- 1.0 to 48+/- 10Mpa. The figure below summarizes the results by Kumar et al.

Table 2.6: Tests results from Kumar et al. [6]

	Tensile Strength	Tensile Modulus	Elongation to Break	Compressive Strength
Sample	GPa	MPa	%	MPa
PP-Control	570 +/- 70	7.1 +/- 0.9	23 +/- 5	25 +/- 1.0
PP + 5 % Nanofiber	491 +/- 60	4.6 +/- 0.8	16 +/- 2	48 +/- 10.0

This study shows the positive effect of fillers to the structural properties of the composite material. The next study will show the inter-relation between the conduction and structure.

Gordeyev et al. made similar fibers, again using polypropylene and short vapor grown carbon fibers [19]. However, the composite fibers were loaded at 0, 5, 10, and 15% volume fraction and tested for tensile strength, Young's Modulus, and DC resistivity. The following figure gives tables that show the results of their experiments.

Table 2.7: Results from Gordeyev et al. [19]

Properties of the drawn composites

VGCF volume fraction (%)	Total draw ratio	Tensile Strength (Mpa)	Young's modulus (GPa)	Strain at break (%)	DC resistivity (m)
0	15	530	8.3	23.7	$>10^{13}$
5	15	720	14.9	20.3	$>10^{13}$
10	15	540	14.1	9.3	$5.3*10^{9}$
15	12	310	11.2	6.9	$5.2*10^{1}$

Table 2.8: Results from Gordeyev et al. [19]

Processing conditions and properties of the as spun composites

VGCF volume fraction (%)	Spinning Temperature (^{o}C)	Draw Ratio	Tensile strength (MPa)	Young's modulus (GPa)	DC resistivity (Ω m)
0	220	1.0	17.2[a]	1.1	$>10^{13}$
0	220	1.5	17.7[a]	1.2	$>10^{13}$
0	220	3.5	24.5[a]	1.8	$>10^{13}$
5	220	1.0	49.3[a]	3.2	$6.2*10^{9}$
5	220	1.5	53.7	3.5	$3.5*10^{10}$
5	220	3.5	77.1	6.3	$1.1*10^{11}$
10	220	1.0	54.0	4.2	$6.8*10^{-1}$
10	220	1.5	57.6	4.7	$1.2*10^{0}$
10	220	3.5	45.1	5.2	$1.0*10^{1}$
15	220	1.0	56.2	4.9	$2.2*10^{-2}$
15	220	1.5	62.4	5.4	$6.0*10^{-2}$
15	220	3.5	42.4	4.6	$9.3*10^{-2}$

[a] stress at yeild point

As shown by the tables, reinforcement strength and stiffness have a maximum effect on the composite fibers at 5% volume loading with a draw ratio of 3.5. Here, the tensile strength increased to 77.1 MPa and stiffness or Young's modulus to 6.3 GPa. The percolation threshold was reached for the composite fibers at some load between the 5% and 10%. This is evident by the large decrease in DC resistivity from greater than 10^{13} (Ωm) at 5 % to $9.3*10^{-1}$(Ωm) at 10%. In fact, the resistivity continued to decrease, as the polymer became more orientated at the higher draw ratios. It was found that the optimum combination for structural and conductive purposes was at 15% volume fraction with a draw ratio of 12 would produce a fiber with tensile strength of 310Mpa, Young's modulus of 11.2 GPa, 6.9 % strain at break and a DC resistivity of 52(Ωm) (2).

Polypropylene

Polypropylene's molecular formula is $(CH_2\text{-}CH\text{-}CH_3)n$. It can assume isotactic, syndiotactic, or atactic configurations. Only the atactic form is used in fiber production because it allows the chains to pack closely to form crystals. The Ziegler-Natta catalysts developed in the 1950s made the atactic formation possible. While polypropylene fibers were first manufactured in Italy in 1957 and U.S. production began in 1962, these fibers did not truly thrive until the 1970-80s, when antioxidants and thermal and ultraviolet stabilizers overcame the polymer's susceptibility to oxidation and radiation induced degradation. The following table summarizes typical properties of textile grade polypropylene fibers.

Table 2.9: Properties of Polypropylene Fibers [20]

Tensile Strength (gf den-1)	3.5-5.5
Elongation (%)	40-100
Abrasion Resistance	Good
Moisture Absorption (%)	0-0.05
Elastic Recovery (after 30s at 2% elongation) Immediate (%) Delayed (%)	 91 9
Glass Transition Temperature (^{o}C)	-15 to –20
Softening Point (^{o}C)	140
Melting Point (^{o}C)	165
Chemical Resistance	Generally Excellent
Relative Density	0.91
Thermal Conductivity	6.0 (with air as 1.0)
Pyrolytic Stability (^{o}C)	350
Electrical Insulation	Excellent
Resistance to Mildew, Moth	Excellent

In textile applications, the typical melt flow rates range between 15-25 g/10min, corresponding to moderate molecular weights, are used [20]. High molecular weights in the range of 3-5 g/10min are used in more technical applications [20]. The polydispersity ranges from 2-12 or greater [20]. A 3 is considered ideal for high speed spinning [20].

Melt Spinning Processing of PP Fibers

Beginning in 1940 with the commercial production of nylon 66, melt spin processing of fibers has proved to be an efficient, cost effect method to produce high quantity and quality fibers. Today it dominates all other fiber forming technologies.

Melt spin processing begins with the feeding of polymer chips (or melt in a continuous process) into the extruder. There are multiple designs/configurations for extruders. Usually a single or twin screw encompassed in a barrel is used to melt the polymer chips and transport the melt along the length of the barrel under pressure. Melting is achieved not only through the heating of the screw and barrel but by the mechanical shearing of the polymer. As the diameter of the screw decreases, the melt becomes more mixed and compressed. The polymer's viscosity during processing is affected by its molecular weight and by the temperature and pressure within the system. Polymer melts experience shear thinning; as the shear rate increases, the viscosity of the polymer decreases.

The polymer passes through a pre-filter before entering the spinning head. The pre-filter is composed of sand particles ranging from 20-80 microns held in place by a series of stainless steel, gauze-like screens of different sizes [20]. Filtration removes partially degraded polymer gels, foreign matter such as metal particulates, and gaseous bubbles. After filtration, the polymer enters the gear pump which tightly measures exact amounts of polymer and releases them into the spin pack. After passing through another filter of fine sand or alumina held in place by metal sintered disks, the polymer finally reaches the

spinneret. The spinneret is a metal plate, 3-30 microns thick with various size holes that influence the size and shape of the spun fibers [20].

Upon exit from the spinneret the melt experiences die swell, a phenomenon where the polymer recovers its stored elastic energy after being released from the high-pressure confinement of the spin pack. The melt is now in the quench chamber, where it is cooled and wound onto a package.

Important Factors

The factors that influence a spun fiber's orientation in order of decreasing impact are: polymer material, extrusion temperature, take up velocity, mass output rate (through put speed), cooling conditions, spinneret channel dimensions, number of filaments, and the spinning path [20]. Typical extrusion temperatures for polypropylene range from 230-290^{o}C, well above the average melting temperature of 165 ^{o}C [20]. Typical take up speeds for PP range from 100-4000 m/min depending on the length of the quench chamber [20].

The relationship between spinning conditions and spun orientation is important because a fiber's molecular orientation, crystallinity, and morphology are directly responsible for a fiber's mechanical and electrical properties. How the melt is stretched and cools along with the crystallization kinetics of the polymer determines if crystallization takes place during spinning.

Crystallinity in a fiber is influenced by its crystallization rate and cooling conditions. The rate of crystallization for polypropylene is very fast. Polypropylene has three crystalline geometries, which can form, depending on the processing conditions: α monoclinic, β hexagonal and γ triclinic. The crystalline phases co-exist with the amorphous phase. Polypropylene can also display a "smectic" form that is an intermediate phase between the amorphous and crystalline. The following figure shows the results of an X-ray diffractogram for polypropylene with different crystals.

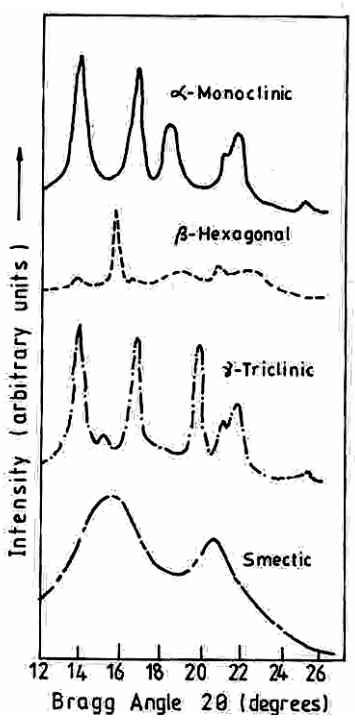

Figure 2.5: X-ray diffractogram of polypropylene crystal structures [20]

Spinning speed affects the geometry of the crystals formed; the greater the speed, the greater the tendency to form the more stable crystalline structures. The following figure shows the tendency to form the α monoclinic crystal form, which is the most stable configuration for polypropylene.

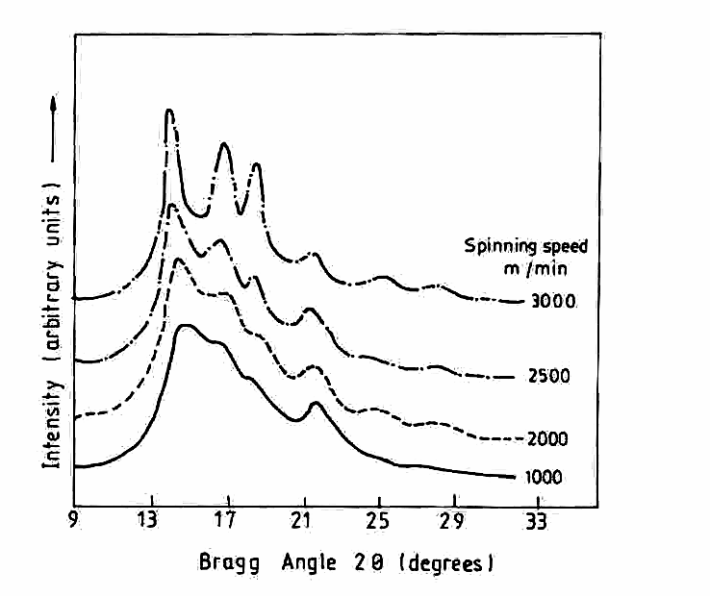

Figure 2.6: Crystalline structure at different spinning speeds [20]

Similarly, plotting the crystalline orientation function of polypropylene verses take up velocity, shows how the orientation of crystals on each axis changes as the take up speed increases. See figure 2.7. f_C represents the axis parallel to the fiber axis. f_b represents the axis perpendicular to the fiber axis and f_a represents the axis 45 degrees to the fiber axis. In terms of fiber morphology, this accounts for the change in formation of spherulitic crystals to row nucleatated with twisted lamenllae to, finally, row nucleated with untwisted lamellae.

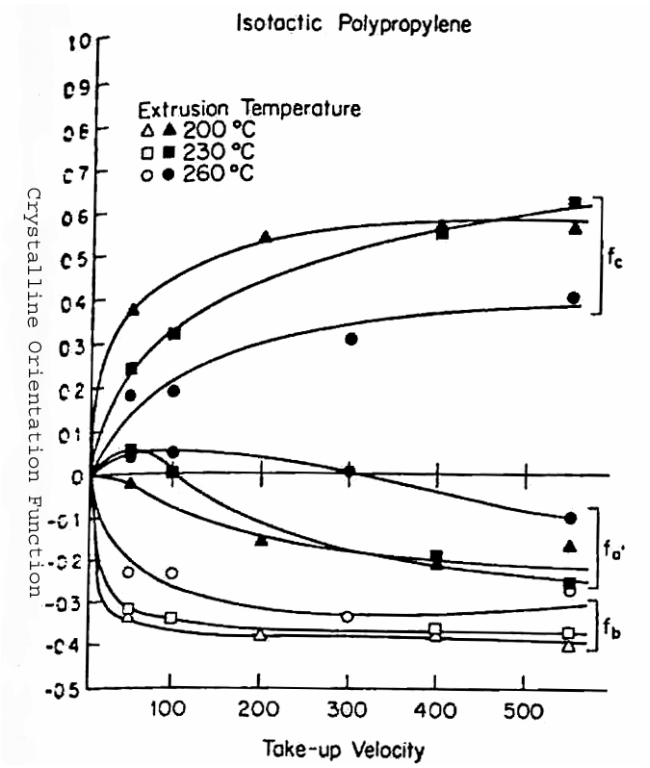

Figure 2.7: Effects of Temperature and Take-Up Velocity on the Crystalline Orientation Function of Polypropylene [20]

Figure 2.8 shows how the mechanical properties of polypropylene are affected by take up velocity. As take up velocity increases, the tenacity of the fibers decreases, while the percent elongation to break increases. It suggests that for this particular fiber and spinning conditions, the 1000m/min take up velocity produces the best fiber.

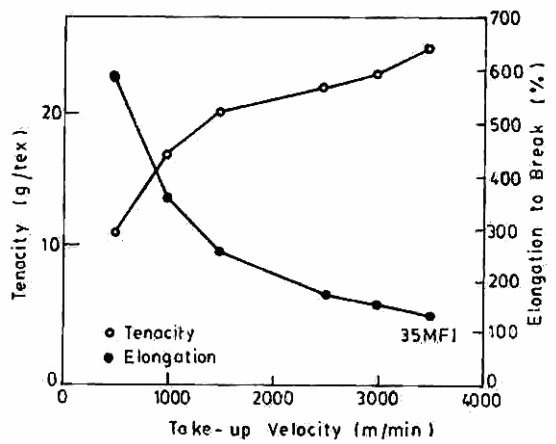

Figure 2.8: Effect of Take-Up Velocity on Fiber Mechanical Properties [20]

Chapter Three

Experimental Approach

3.1 Materials

Fibril™ carbon nanotubes pre-compounded in Equistar 51S30VPP, 30 melt flow rate polypropylene, were purchased from Hyperion Catalysis International at 15% by weight concentration. Equistar 51B30V, 30 mfr PP, was purchased from Performance Polymer to create control and dilutions. Sunoco CP360H, a 34 mfr polypropylene was also used for comparison in the early testing of the polymer.

3.2 Equipment

Mini Lab Micro Rheology Compounder
Manufacturer: Thermo Haake
Purpose: characterize polymer rheology

Meltflixer
Manufacturer: Thermo Haake
Model: MT
Purpose: determine polymer melt flow rate

Polymer Compounder
Manufacturer: Leistritz
Model: LSM 34 GL
Purpose: mix polymer and additive (CNT)

Single Screw Extruder
Purpose: spin fibers

Vibromat
Manufacturer: Textechno
Model: ME
Purpose: determine fiber linear density

MTS
Manufacturer: MTS ReNew
Model: 1122
Purpose: Tensile Tester

Optical Microscope
Manufacturer: Nikon
Model: Labophot-pol
Purpose: View polymer smears and fibers

Digital Camera
Manufacturer: Nikon
Model: D1x
Purpose: Photograph polymer smears and fibers

Scanning Electron Microscopy
Manufacturer: Hitachi
Model: S 3200N
Purpose: Image fibers

Circuit
Manufacturer: N/A
Model: N/A
Purpose: Test fiber conductivity

3.3 Procedure

3.3.1 Initial Characterization of the as received 15% CNT Polypropylene

To determine how the compounded polymer would react during spinning some initial tests were preformed to characterize the polymer. The Mini Lab was used to examine the polymer response to different temperatures and shear rates under a nitrogen purged environment. The three temperature tested were 196^{o}C, 230^{o}C, and 290^{o}C, and the three shear rates tested were 65, 135, and 210. The sample size was 5 grams.

Tests with the Meltfixer, an instrument used to determine melt flow rate, mfr, was performed according to ASTM D 1238, Standard Test Method for Melt Flow Rates of Thermoplastics by Extrusion Plastometer E (2002). The material was tested as received from the supplier in pellet form at a temperature of 230 ^{o}C under a 2.16Kg weight using procedure B of the standard. Sample size was 7 grams.

3.3.2 Trial I: Spinning

In the first trial controls of 100% polypropylene were spun where the temperature, take up velocity, and orifice diameter were varied to characterize the behavior of the virgin polymer. The virgin PP was then loaded with the 15% CNT / PP into the single screw extruder and a let down of 0.5% CNT/PP was spun. The spinning conditions and details for Trial I are listed in Appendix I.

3.3.3 Compounding Polymer

To address the issue of inadequate dispersion that arose in the first trial, the virgin PP and 15% concentrate were taken to Ameri Chem, Concord, NC, where a 34mm Leistritz LSM 34 GL twin screw extruder, 1230 cm long, was used to compound the polymers into 0.5%, 1.0%, 1.5%, 2.0%, and 3.0% concentrations. The polymers were compounded at 130 rpm at 400^{o}F (204.4^{o}C) into a cold water bath, and then pelletized.

3.3.4 Characterization of Compounded Let downs

Further tests with the Meltfixer were run to determine the melt flow of the different polymer concentrations according to ASTM D1238. Three samples per treatment were tested. Again, the polymer was in pellet form and run at a temperature of 230 ^{o}C under a 2.16Kg weight using procedure B of the test method.

Polymer smears were made on glass sides by heating small amounts the polymer to melt and then pressing them with glass cover slips to spread the material over the slide. The slides were examined at 60X magnification using the Nikon Labophot-pol optical microscope. The Nikon D1x digital camera was mounted to the top of the microscope and used to photograph the slides. The digital images were examined to view particulate sizes with the knowledge that this would provide only a rough estimate due to distortions in particle size from the cover slide and preparation technique.

3.3.5 Trial II: Spinning

A second attempt at spinning using the twin screw compounded PP yielded greater success. Fibers that contained up to 0.5%, 1.0%, 2.0%, and 3% CNT were spun. Bicomponent fibers at 1% CNT core loading were made in the following sheath/core ratios: 60/40, 40/60, and 20/80. Bicomponent fibers at 3.0% CNT core loading were made in the following sheath/core ratios: 70/30, 50/50, and 20/80. The spinning conditions and details are listed in Appendix II.

3.3.6 Fiber Testing

Optical Microscope

Fibers were placed on glass slides and then viewed under the microscope. The Nikon D1x was used to photograph the fibers at 10x magnification.

Scanning Electron Microscope

Small pieces of fibers were cut and mounted on double sided carbon tape which was mounted on the microscope's stage. The stage was then loaded into the machine and digital images were recorded.

Linear Density

The fibers' linear density in denier was determined using the Vibromat according to ASTM D 1577-01, Standard Test Method for Linear Density of Textile Fibers: Option C Vibroscope. The sample size was increased from ten to twenty fibers due to large variations in fiber diameters.

Mechanical Testing

The fibers' mechanical properties were determined using the MTS outfitted with fiber grips according to ASTM method D 3822-01, Standard Test Method for Tensile Properties of Single Textile Fiber. A one-inch gauge length and 1N load cell was used for all fiber samples with the exception of the 3% fibers, where a 10 N load cell was used. Fiber slippage was encountered when using the fiber claps. In order to overcome the slippage, fibers were first mounted on index cards cut in the shape of the block letter C

and secured with masking tape. The gap in the letter measured one inch. Notches were cut on the outer side of the letter and the fiber was wrapped around the card on the top and bottom. The fiber was further secured with more masking tape. Care was taken not to stretch the fiber during this process.

Conductivity

The fibers' conductivity was tested in accordance to a modified version of ASTM D 257, Standard Test Method for DC Resistance or Conductance of Insulating Material. The circuit depicted below was used to test the fibers at 500V for 60second over a fiber length of one inch. The circuit is constructed of a Fluke-77 multi-meter, a High Voltage Power Supply-ES30N by Gamma High Voltage Research, a Radio Shack Bread Board, wire and a resistor of 10 *100K ohms with a tolerance of 5%.

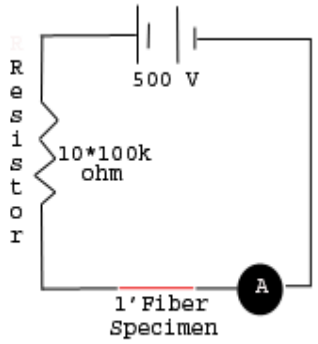

Figure: 3.1: Series Circuit Diagram

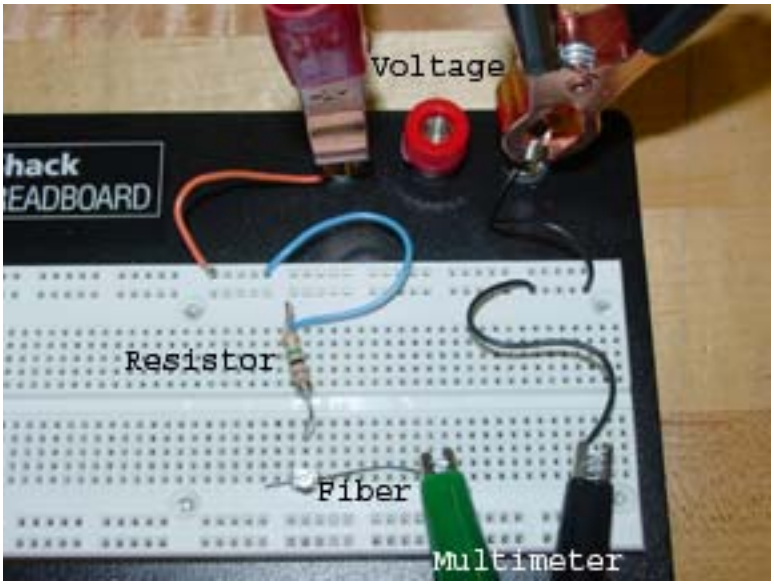

Figure 3.2: Series Circuit

The circuit is built in series. Using Ohm's law, V = IR, calculating the resistance is simple. The current, I, is the same throughout the circuit and is read off of the multi-meter which is set to read amps. The voltage sum, V, is 500V. The resistances, R, is additive where the R equals sum of 10*100K ohms plus the resistance of the fiber.

Chapter Four

Results and Discussion

The initial information gathered from the Mini Lab, figure 4.1, on the 15% concentration shows a very large increase in the viscosity compared to a 34 MFR virgin PP sample. At 230^{o}C the 34 MFR PP has a viscosity that ranges from 58 Pa*s to 46 Pa*s, while the 15% concentration ranges from 459 Pa*s to 158 Pa*s over the same shear rates, 58 1/s, 136 1/s and 204 1/s. The overall behavior of the 15% concentration remains shear thinning. Increasing the temperature decreases the viscosity of the material as expected.

This information is important and useful to know when melt processing the polymer concentrates. The shear thinning behavior of the polymer assures that it will not crosslink during processing and damage equipment. Temperature is positively identified as a means to adjust the viscosity during spinning if necessary.

Thermo Haake Mini Lab Micro Rheology Compounder:

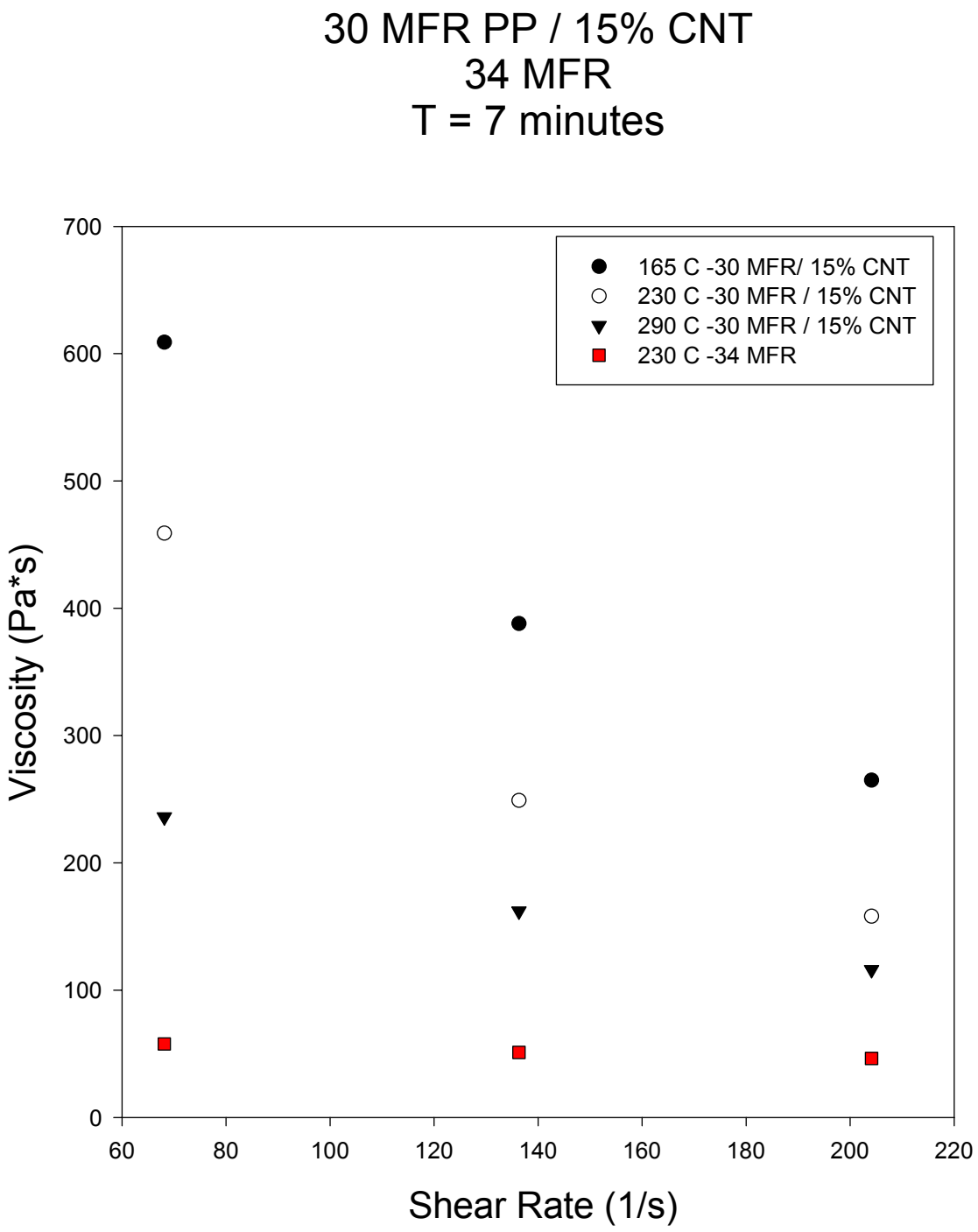

Figure 4.1 Effect of shear rate and temperature on viscosity for 15%CNT / PP material

An initial test on the Meltflixer revealed that the 15% concentration flow rate was too low to be detected by the test. The viscosity data from the Mini Lab combined with the virtually zero melt flow rate for the 15% concentration signified that spinning at this concentration would not be possible. In order to process the 15% concentration it must be diluted.

Figure 4.2 shows the melt flow rate decreased from 30 to 10 as the concentration of carbon nanotubes increased from 0 to 3%. This confirms that the polymer let downs made were fluid enough to spin with conventional equipment. It was also revealed that spinning with carbon nanotube concentrations greater than 3% would be very difficult because the melt flow rate becomes so low that the polymer no longer flows freely. A possible way to increase the CNT concentration in future research is by using a higher melt flow rate material initially.

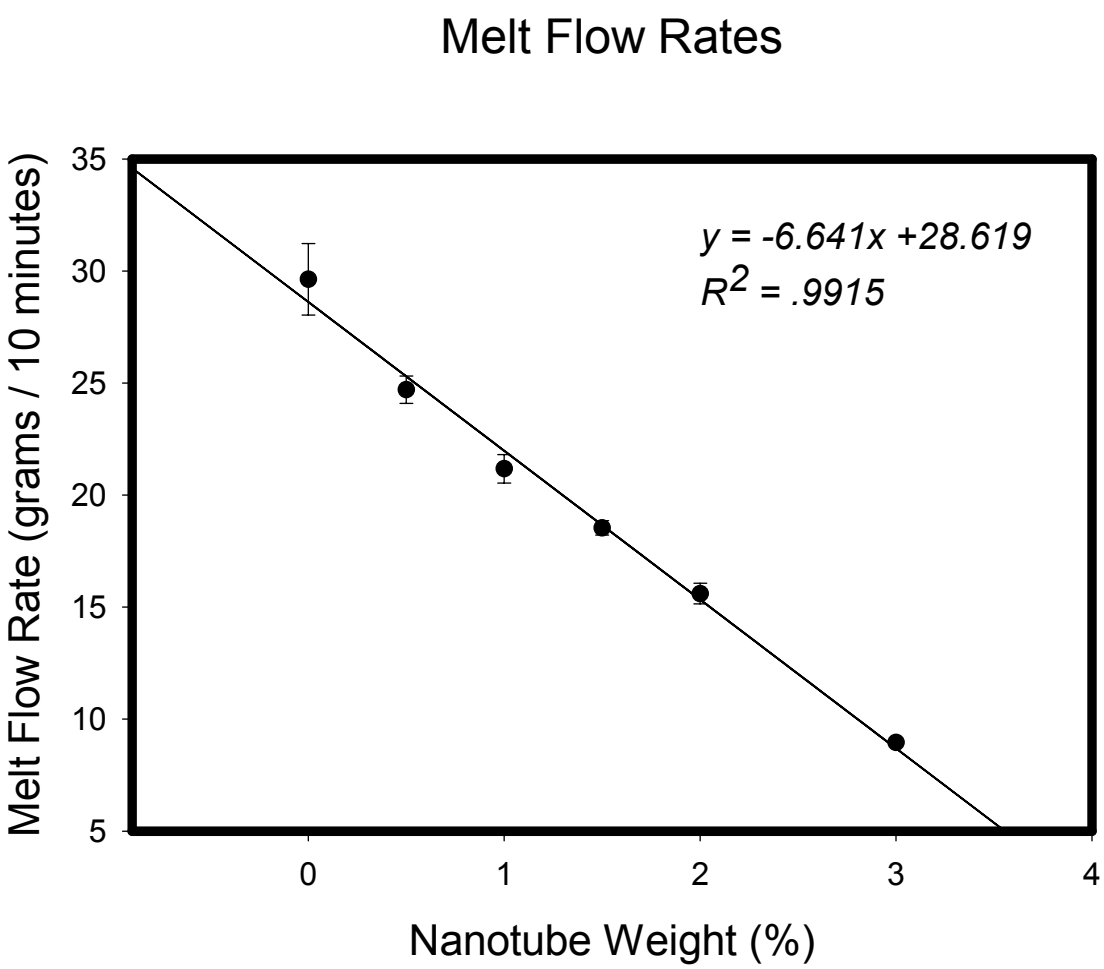

Figure 4.2 Effect of increasing nanotube concentration on melt flow rate

The polymer smears allowed a look at the distribution of carbon nanotubes within the polymer, as seen in figures 4.4-4.9. Increases in the concentration of nanotubes decreased the overall opacity as expected. At the lower concentrations, figure 4.4-4.7, the formation of agglomerates is very evident and the aggregates can be distinguished from each other. At higher concentrations, figures 4.8-4.9, it is more difficult to separate the aggregates.

Compounded Polymer Smears:

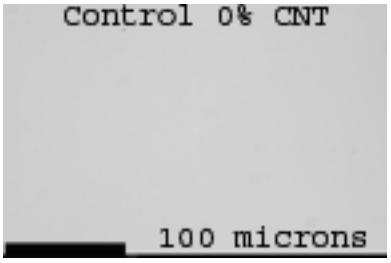

Figure 4.3 Smear photograph at zero CNT concentration

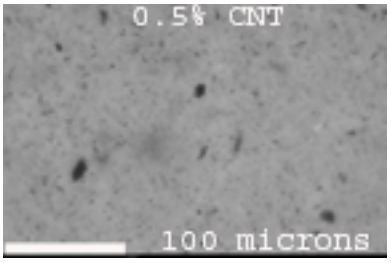

Figure 4.4 Smear photograph at 0.5% CNT concentration

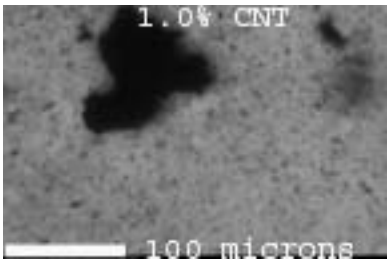

Figure 4.5 Smear photograph at 1.0% CNT concentration

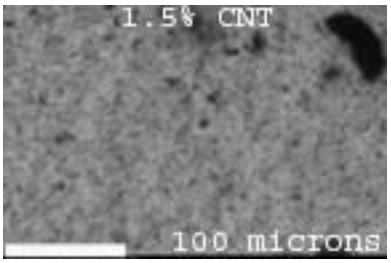

Figure 4.6 Smear photograph at 1.5% CNT concentration

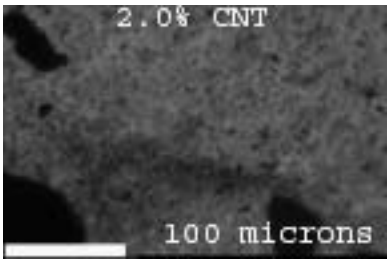

Figure 4.7 Smear photograph at 2.0% CNT concentration

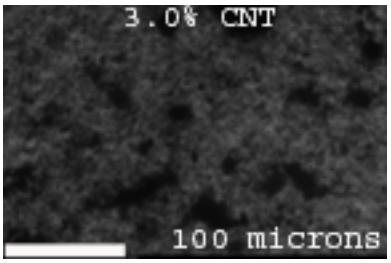

Figure 4.8 Smear photograph at 3.0% CNT concentration

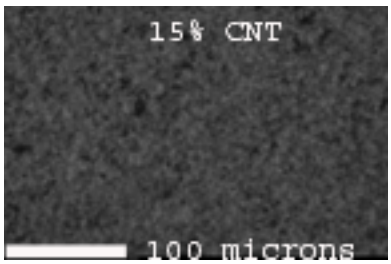

Figure 4.9 Smear photograph at 15.0% CNT concentration

Passing light through the slides to photograph them is very difficult. This is due in part to the increase in viscosity caused by the nanotubes, which makes it difficult to spread the polymer on the slide, and the nanotubes themselves, which absorb the light. In fact, it was only possible to photograph the outer edges of the smears at the higher concentrations. The information on the formation of aggregates, as well as the spinning experience from Trial I, lead to modifications in the spinning filtration, namely the removal of the fine meshes, since the removal of the carbon nanotubes is unwanted. See Appendices I and II for details on spinning filtration used with each fiber.

Figure 4.10 shows that the fiber denier generally increased as nanotube loading increased. However, there is no significant statistical difference between fiber denier for zero concentration and the 1.0% concentration, and no statistically significant difference between the 0.5% concentration and the 1.0% concentration. All other fiber deniers shown in the figure were significantly different. Detailed statistical information for all the composite fibers is located in Appendix III. The differences seen in fiber denier are due to the differences in drawing that the fibers experienced. (The orifice diameter remained constant for all the composite fibers spun in Trial II, 1.5mm.) The 0% , 0.5% and 1.0% fibers were all drawn at 415 m/min while the 2.0% was drawn at 215 m/min and the 0% was not drawn on the rollers at all. These differences in draw ratios in turn affect the mechanical properties of the fibers, as will be show later.

Fiber Denier

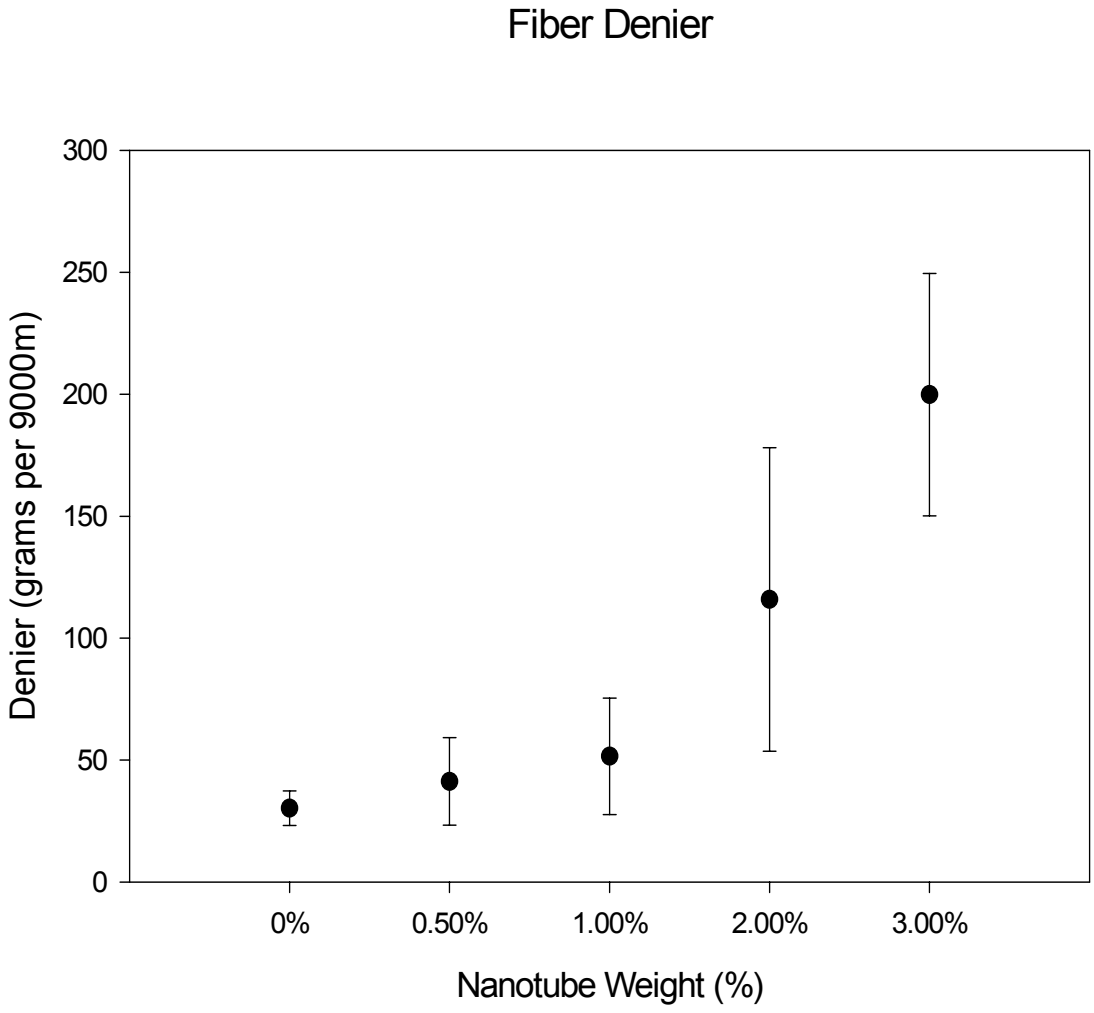

Figure 4.10 Effect of nanotube concentration on fiber denier

Figure 4.11 shows the fiber denier for the 1.0% core bicomponent fibers. There is a statistically significant difference between the 0/100 (the 100% composite fiber at 1% concentration – not a sheath /core configuration) and the bicomponent fibers, 20/80, 40/60, and 60/40. There is no significant difference between the bicomponent fibers. All the fibers were drawn at 415 m/min.

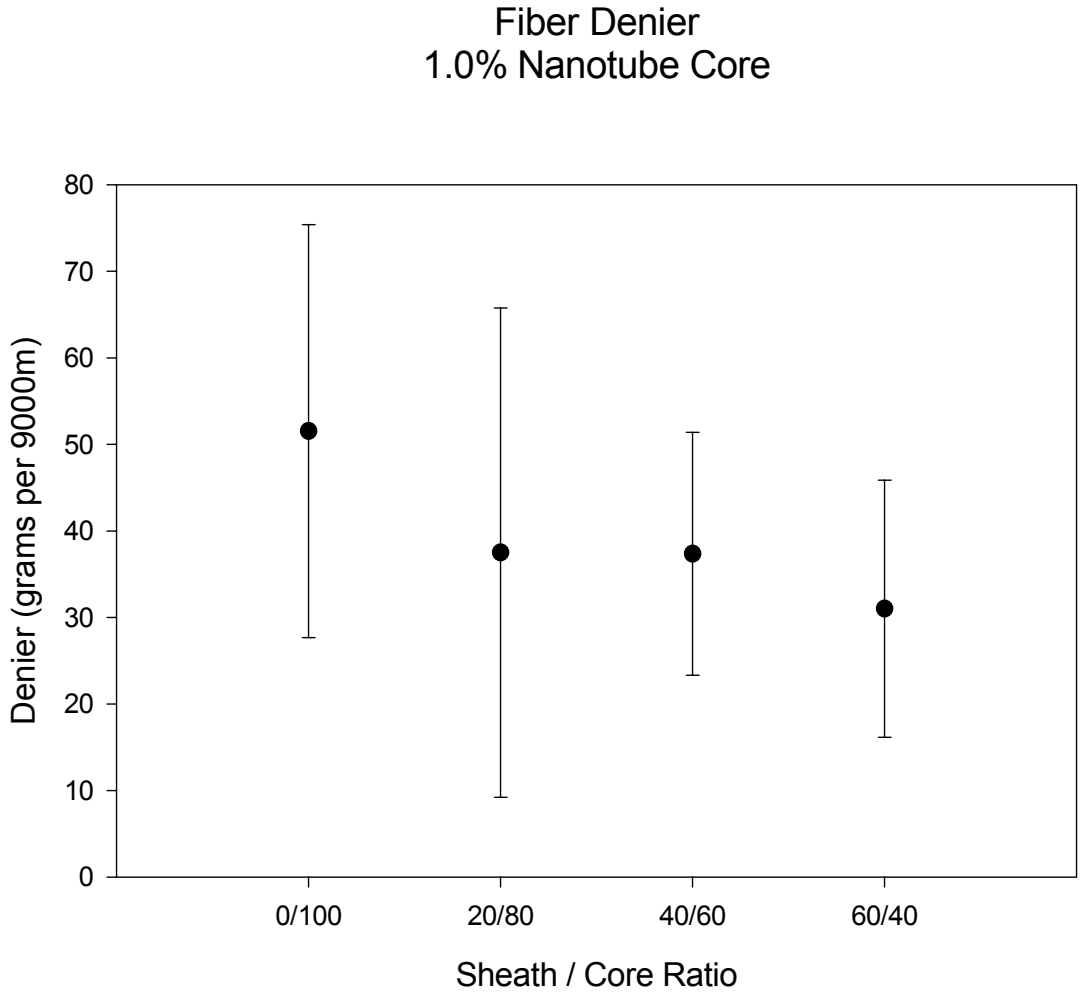

Figure 4.11 Effect of Sheath/Core ratio (1% CNT core) on fiber denier

Figure 4.12 shows the fiber denier for the 3.0% core bicomponent fibers. The fibers show a statistically significant difference in their deniers with the exception of the 50/50 and 70/30 fibers. There is no significant difference between the 50/50 and 70/30 bicomponent fiber deniers. Neither the 0/100, 20/80 nor the 50/50 fibers were drawn onto rollers. The 70/30 was drawn onto a package at 200 m/min. It is unclear why the 50/50 fiber denier is not as large as the 0/100 and 20/80.

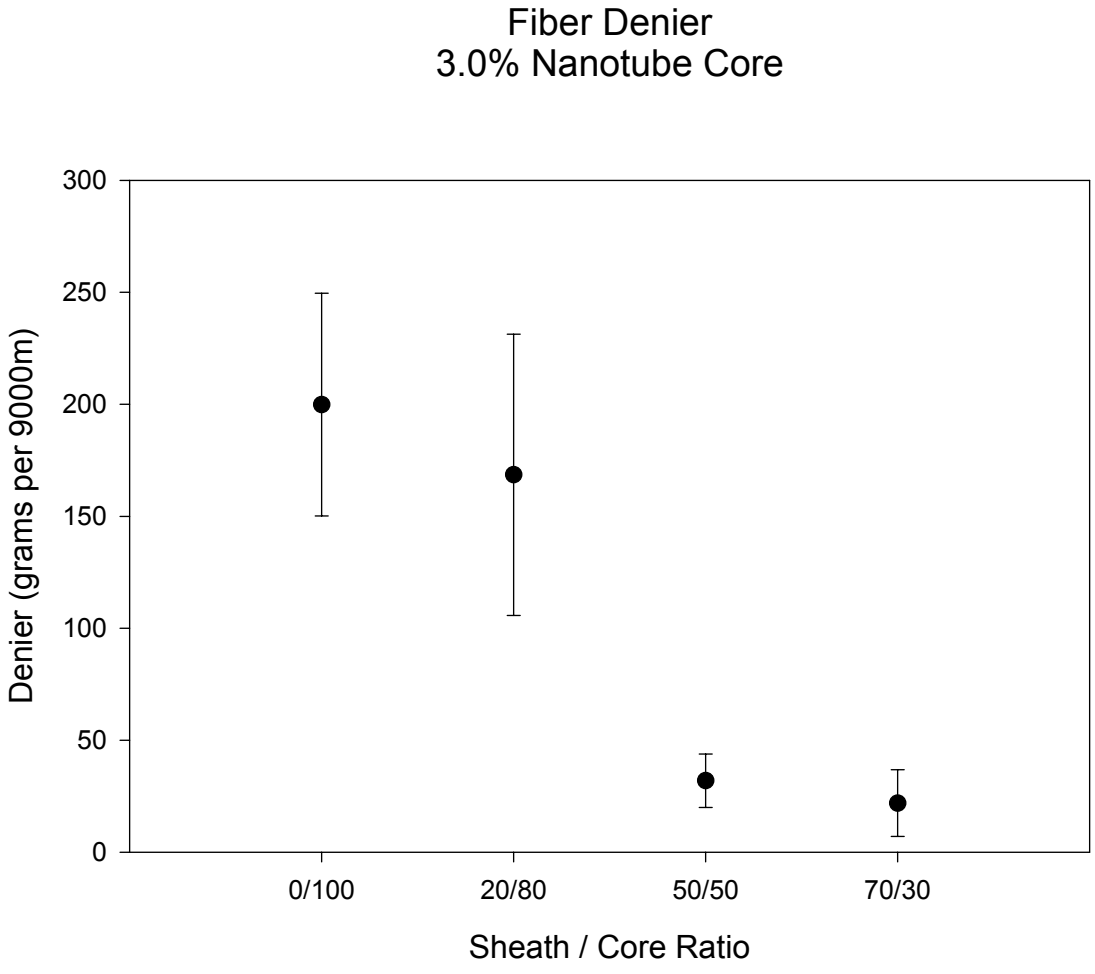

Figure 4.12 Effect of Sheath Core Ratio (3% CNT core) on fiber denier

Increasing denier is due to two effects caused the introduction of the nanotubes: formation of aggregates and higher viscosity, which directly affects the fibers' ability to be drawn. Thus the draw on the fibers had to be modified with nanotube concentration. The carbon nanotubes increase the polymer viscosity, so with higher loading the polymer does not flow as well as with lower loadings. This means that the take-up velocity has to decrease in order to wind the fibers; thus the fibers are not drawn as much and are therefore thicker. Aggregates of nanotubes serve as stress concentration points and can initiate breaks while the fiber is being drawn, also adding to the need to decrease take up speeds during processing. Additionally, the clumping of the carbon nanotubes causes the formation of increasing irregular fiber surface, resulting in areas of locally increased fiber circumference. (Figures 4.22 to 4.26 show this phenomenon with optical micrographs and figures 4.33 to 4.41 show it with SEM micrographs.) Furthermore, as the nanotube loading increases, the fibers tend to stick together more, which adds to difficulty in separating single fibers for testing and indicates a need for changes in the quench conditions in future projects.

Overall, from figure 4.13, as the carbon nanotubes increased, the fiber's breaking strength and strain decreases. However, the 3.0% fibers departed from the group's behavior and exhibited failure with little extension and only a slight increase in fiber strength over the 2.0% and 1.0% fibers. The composite fibers do not exhibit the natural draw that the 100% polypropylene fiber does. The introduction of the nanotubes, and their aggregates, prevent the polymer chains from slipping past each other and leads to stress concentration points and eventually fiber breakage at lower extensions.

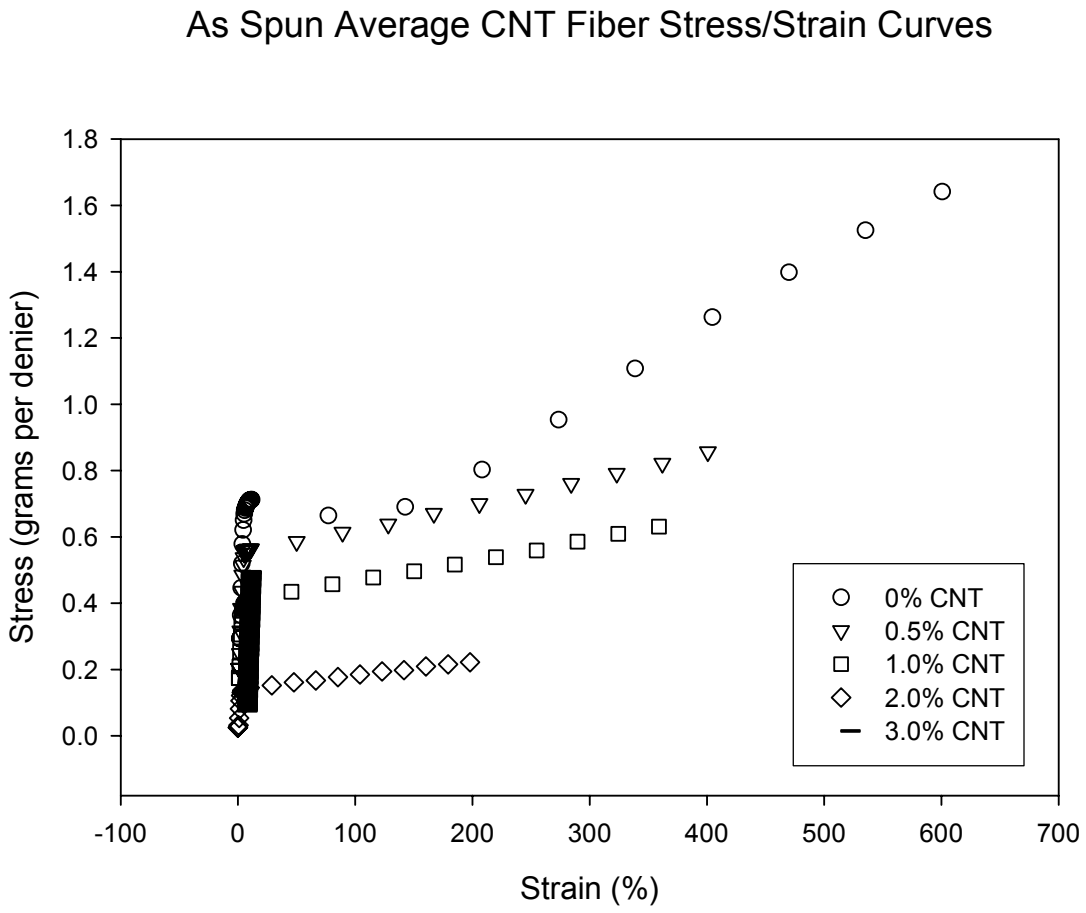

Figure 4.13 Effect of nanotube concentration on Stress / Strain curves

Additionally, it should be mentioned again that the 2% and 3% fibers were not drawn to the same as spun ratio as the control (0%), 0.5%, and 1.0% fibers. The 2% fibers wound on the package at 215 m/min while the 3% concentration fibers were unable to be treaded up on a package at all. (See Appendix II.) The difference in the as spun drawing can contribute to differences in the mechanical properties of the fibers. It makes it unclear which differences in mechanical properties are due to the aggregates and which are due to the changes in the as spun draw. Never the less, the changes in as spun draw were necessary in order to spin the fibers and the changes were due to the introduction of the

aggregates. So, even if the aggregates are not the direct cause of the mechanical differences, they are the indirect cause. Also adding to this confounding of data is temperature fluxations, which also can impact the mechanical properties. (See Appendix II.)

Figures 4.14 and 4.15 follow similar trends, as the amount of CNT in the fiber is increased, that is as the core increased, fiber strength is lost. However the 50/50 and 40/60 fibers appear to exhibited the largest breaking strain.

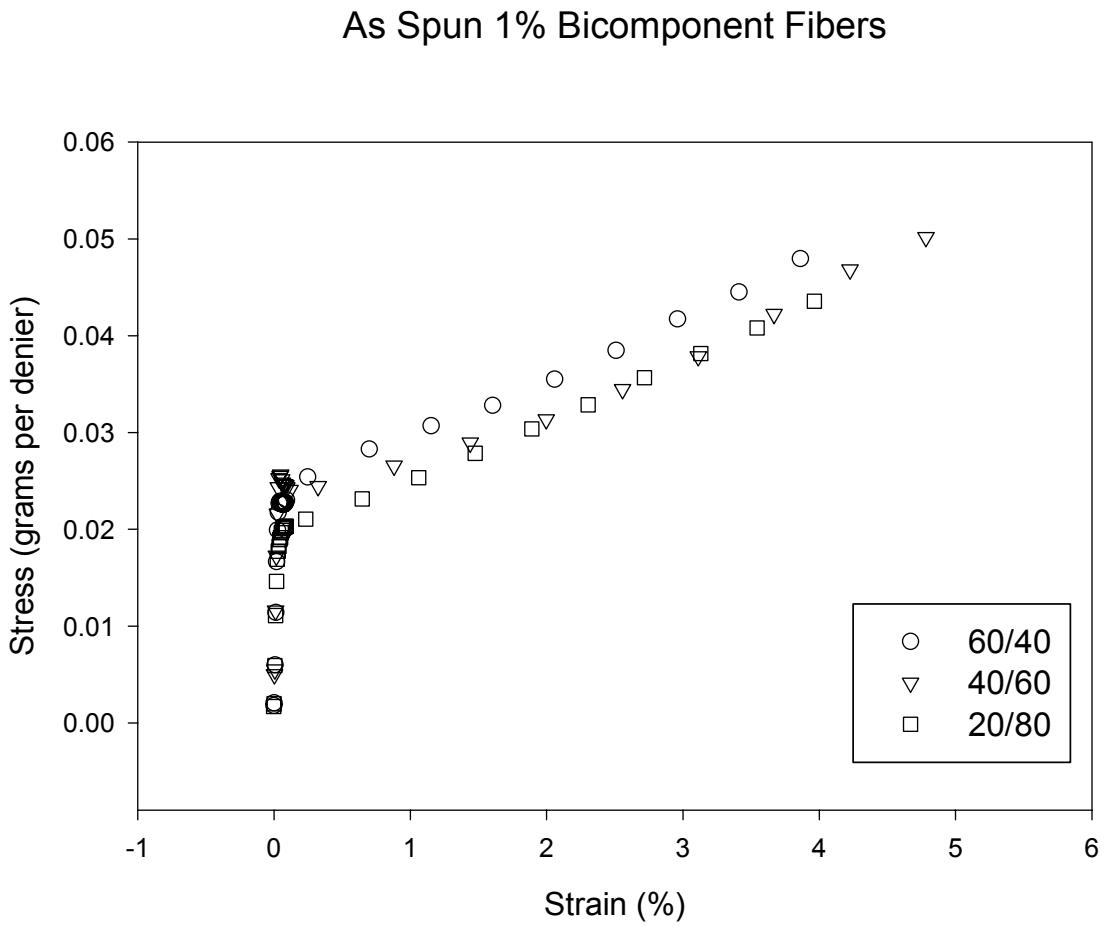

Figure 4.14 Effect of Sheath / Core ratio (1% CNT core) on stress / strain curves

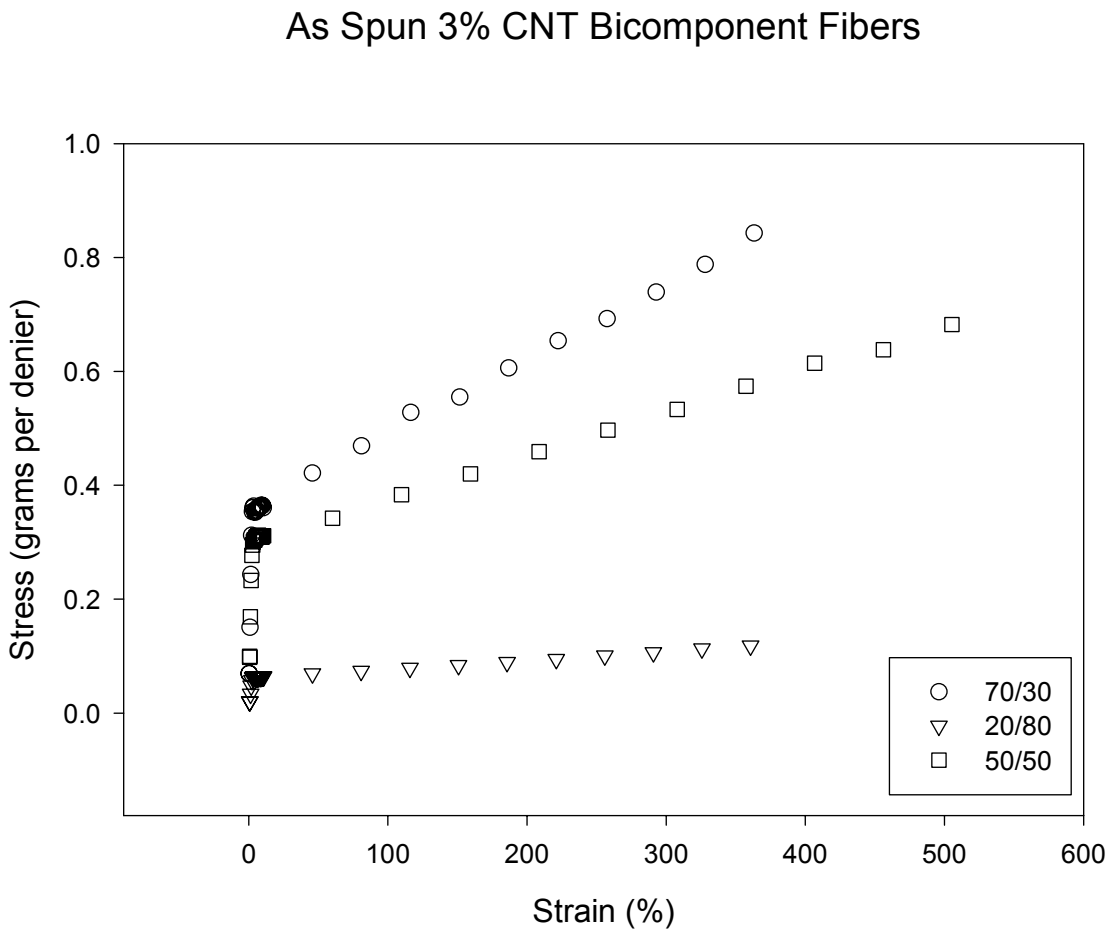

Figure 4.15 Effect of Sheath / Core ratio (3.0% CNT core) on stress/ strain curves

Figure 4.16 shows the breaking stress for the 100% composite fibers as nanotube load increases. All the breaking stresses are significantly different with one exception; the 0.5% concentration and 1.0% concentration, which are the same. The trend for the fiber stress is decreasing as nanotube weight increases, but at 3.0% the stress jumps back up to approximately the same level as the 1.0% fibers. The 3.0% fiber is very different from the others, in that it is very brittle and does not stretch, which is why it requires more force to break.

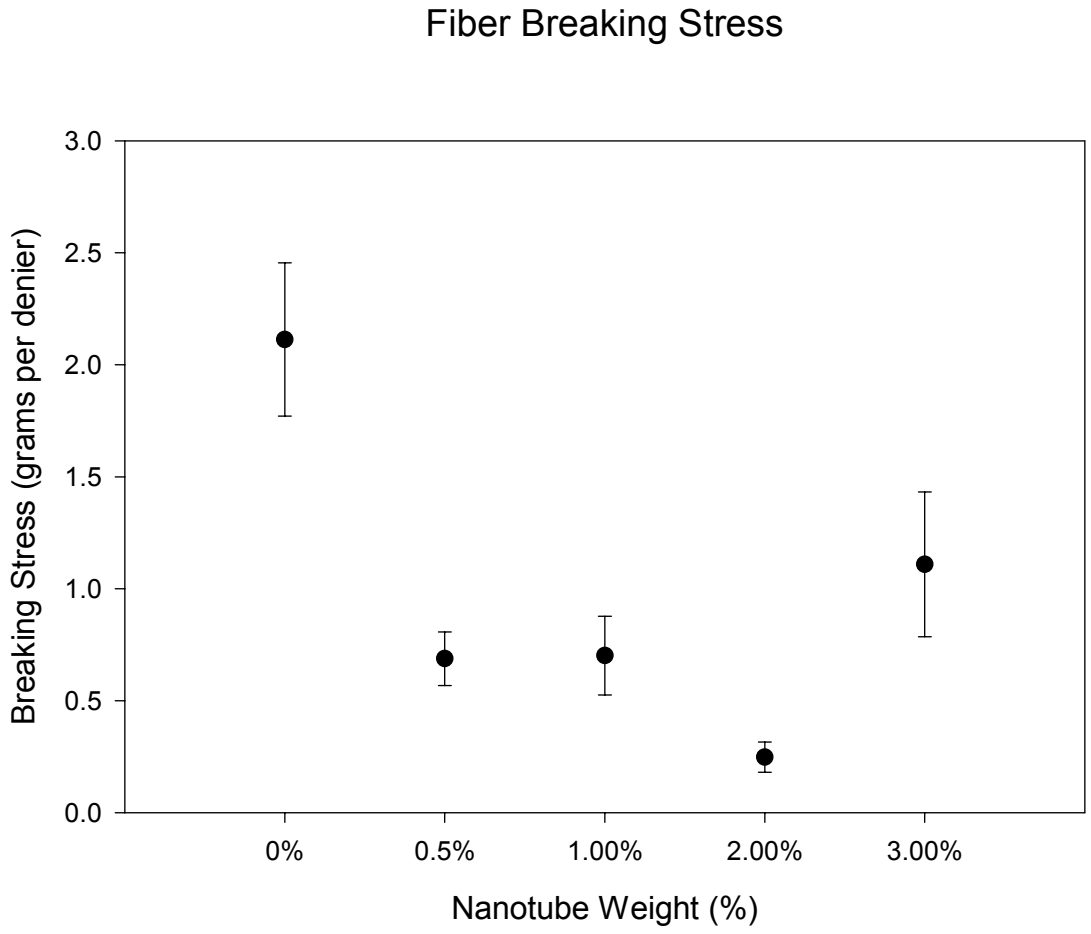

Figure 4.16 Effect of nanotube concentration on stress

Figure 4.17 shows the breaking strain for the 100% composite fibers. The clear trend observed here is that as nanotube load increases, the fiber breaking strain decreases. All values are significantly different with the exception of the 0.5% concentration and 1.0% concentration, which are not significantly different.

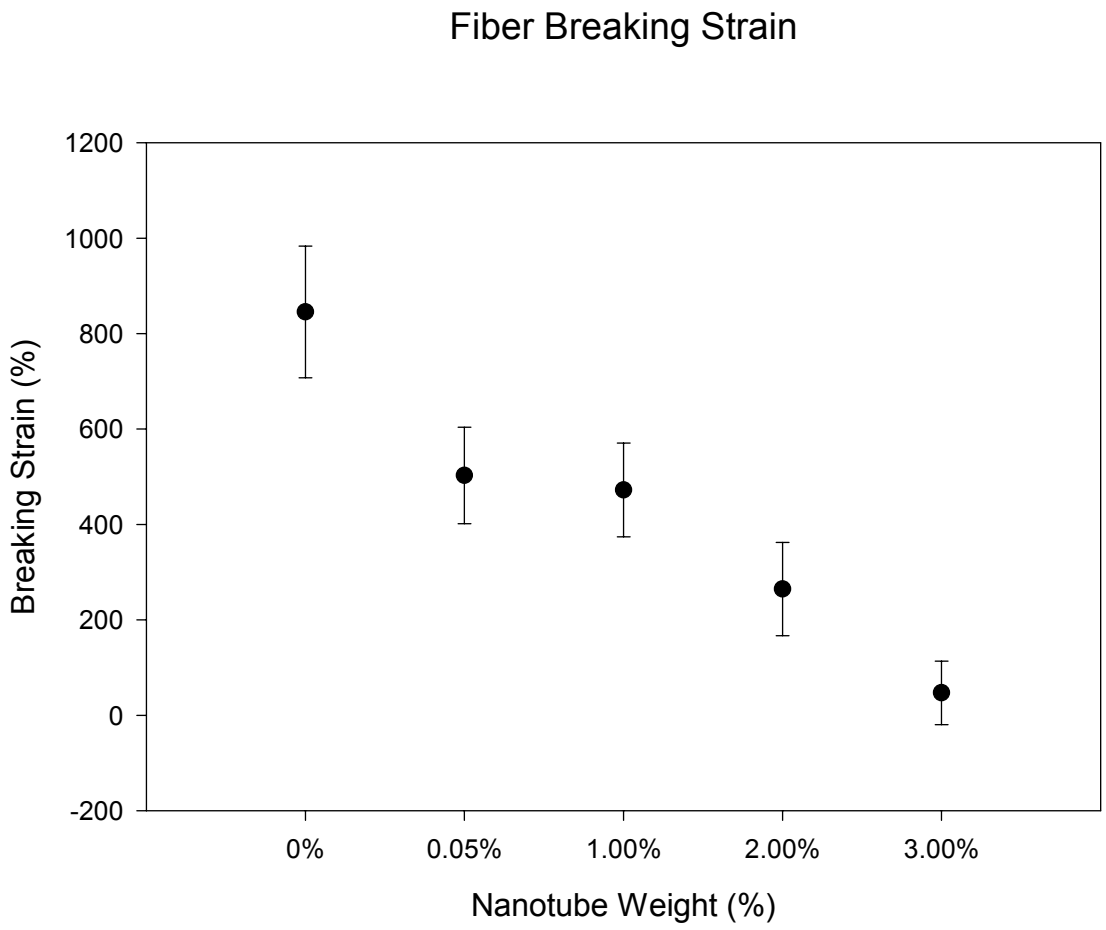

Figure 4.17 Effect of nanotube concentration on % strain

Figure 4.18 shows the fiber breaking stress for the 1.0% bicomponent fibers. The breaking stresses are significantly different between 60/40 and 20/80 fiber and also for the 40/60 and 20/80 fiber, but there is not significant difference between the 60/40 and 40/60.

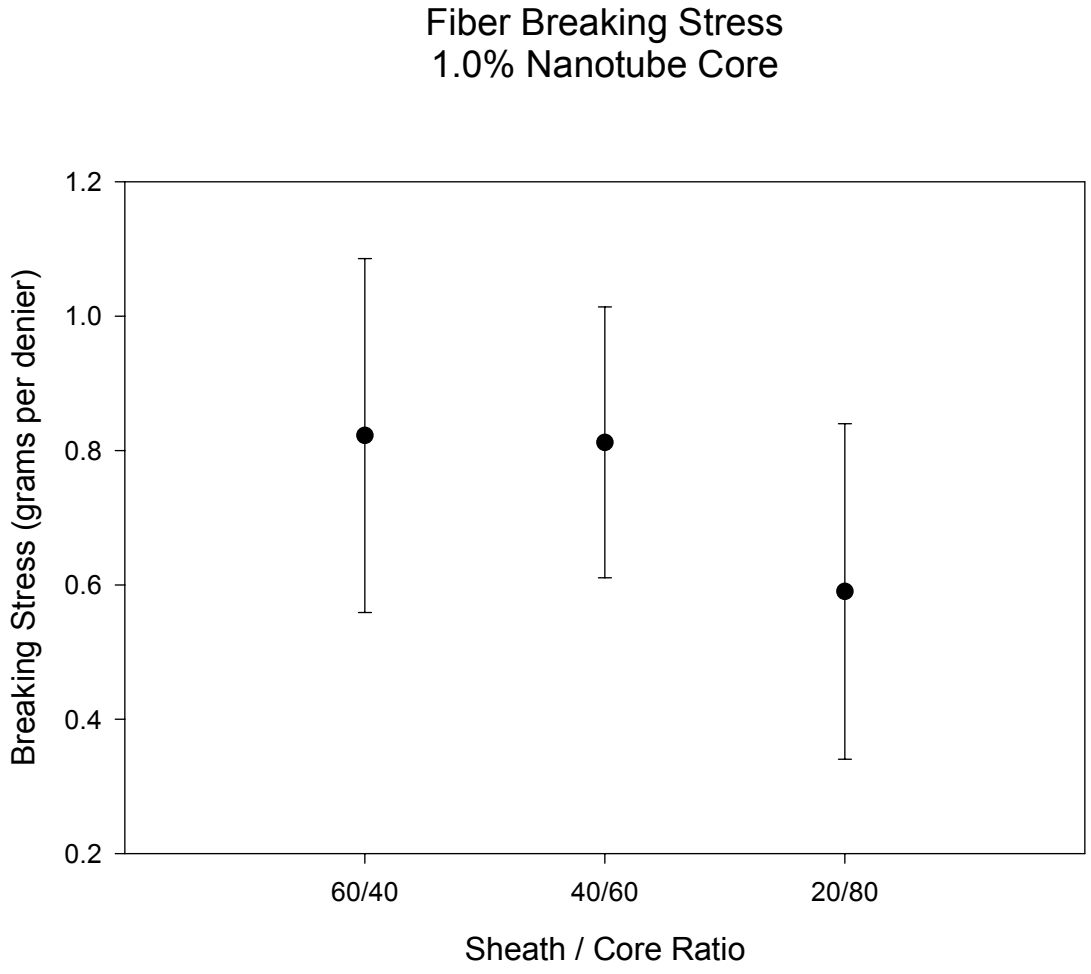

Figure 4.18 Effect of sheath / core ratio (1% CNT core) on breaking stress

Figure 4.19 shows the fiber breaking strain for the 1.0% bicomponent fibers. The breaking strain for the 60/40 and 20/80 as well as the 60/40 and 40/60 are significantly different. However, there is not any significant difference between the 60/40 and 80/20 breaking strains.

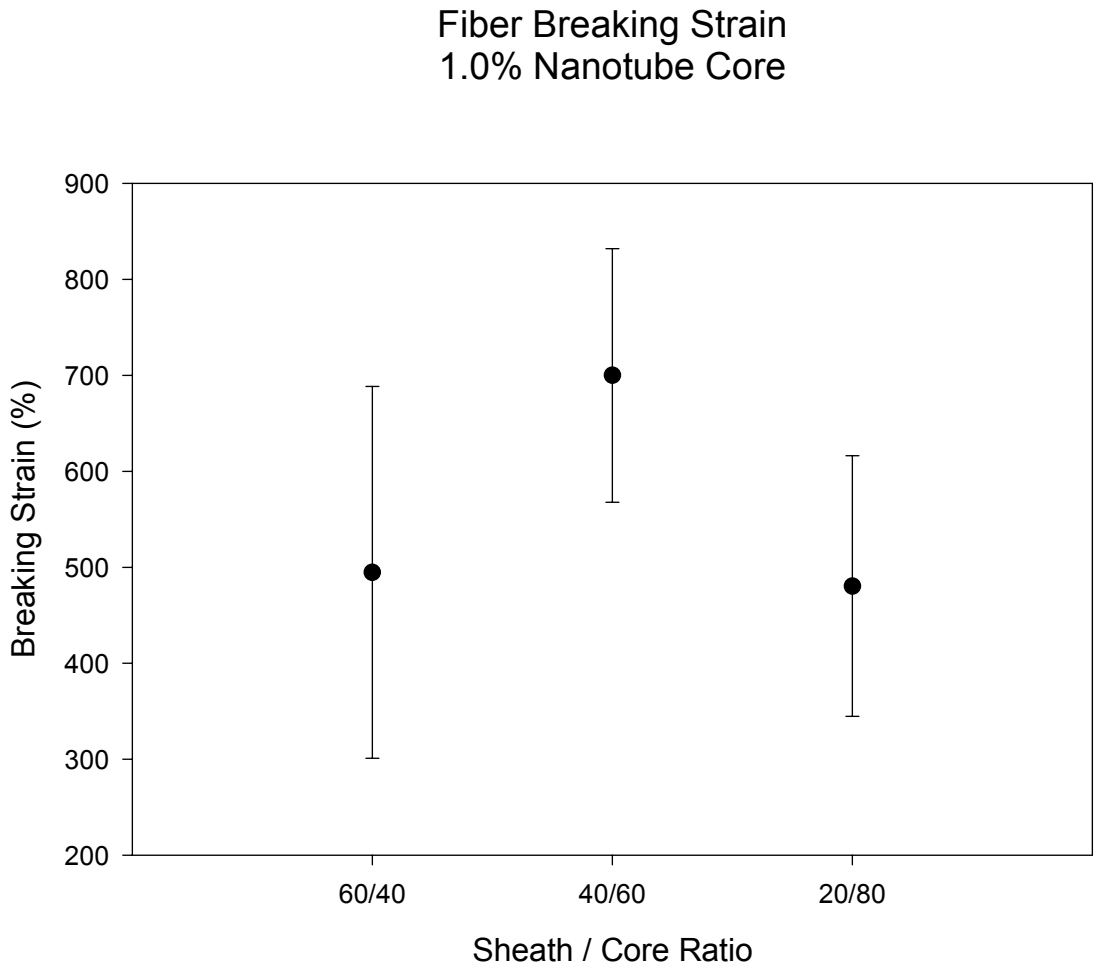

Figure 4.19 Effect of sheath / core ratio (1% CNT core) on breaking strain

.

Figure 4.20 shows the fiber breaking stress for the 3.0% bicomponent fibers. All three fiber groups are significantly different from each other.

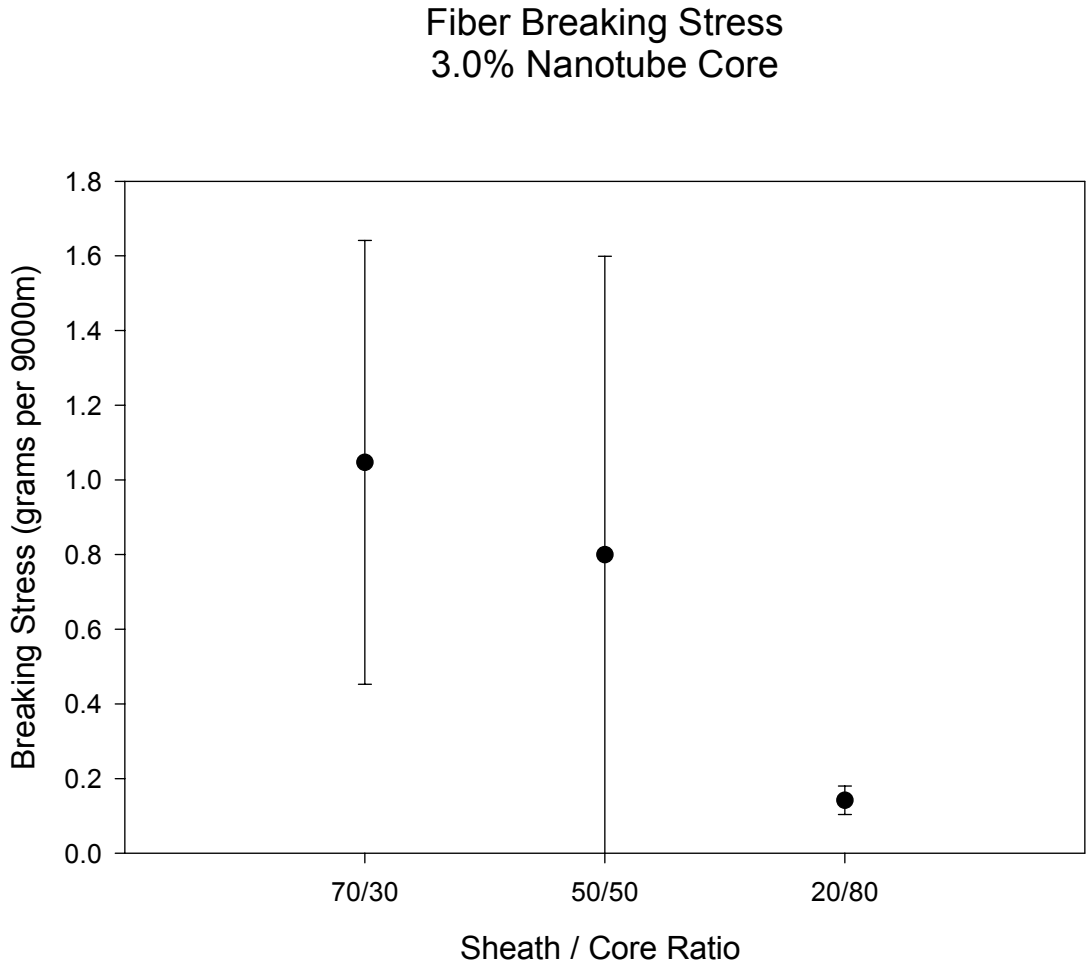

Figure 4.20 Effect of sheath / core ratio (3% CNT core) on breaking strain

Figure 4.21 shows the fiber breaking stress for the 3.0% bicomponent fibers. The 70/30 and 50/50 fiber are significantly different in their breaking stresses, as are the 50/50 and 20/80 fibers. However, the 70/30 and 20/80 are not significantly different.

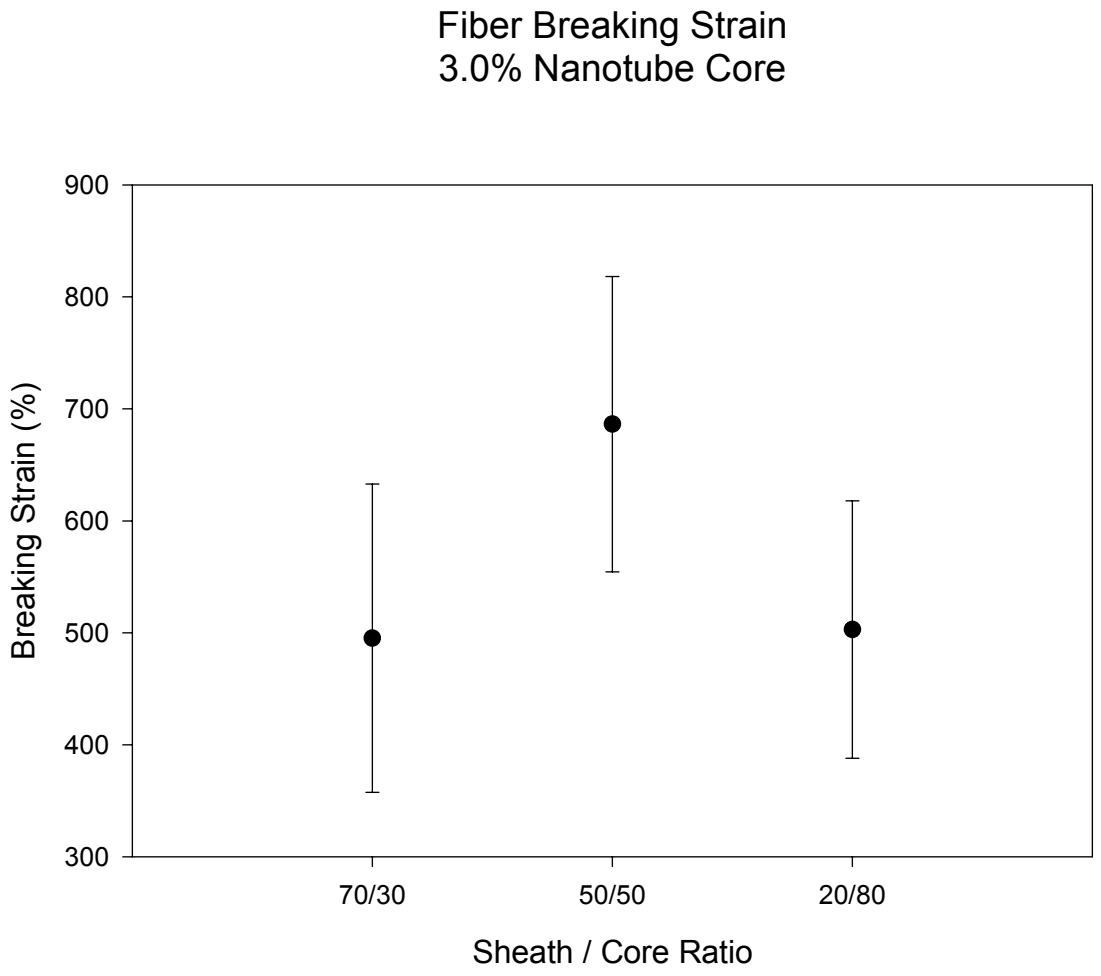

Figure 4.21 Effect of sheath / core ratio (3% CNT core) on breaking stress

The optical microscopy work on the composite fibers showed that the lumps on the fibers were carbon nanotube aggregates within the fiber. The control fibers are smooth along the sheath and colorless, see figure 4.22. As soon as the nanotubes were introduced the color of the fibers turned into a deep charcoal and deepened to a black as the nanotube concentration was increased. The 0.5% and 1.0% concentration are translucent enough to show the rounded carbon nanotube agglomerates within the fiber and on the fiber's surface, see figures 4.23-4.28. It is also evident that at these concentrations the agglomerates are discontinuous along the length of the fiber. The 2.0% and 3.0% fibers do not allow light to pass through them due to the heavier loadings. This suggests that these fibers have a better probability of having reached percolation. The contours of the 2.0% and 3.0% fibers can be seen and the disfiguration is quite evident, as is an increase in fiber diameter, see figures 4.29-4.30.

Optical Microscopy

Figure 4.22

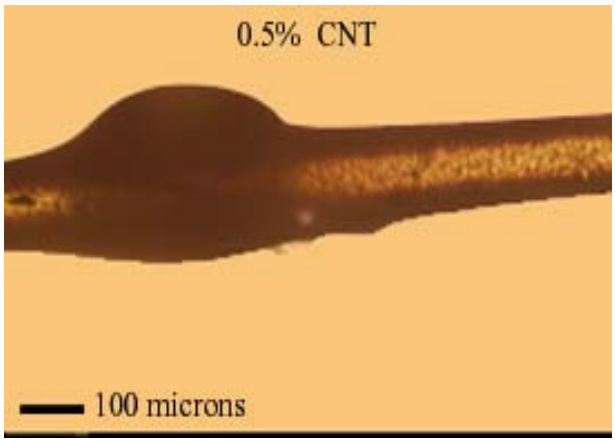

Figure 4.23

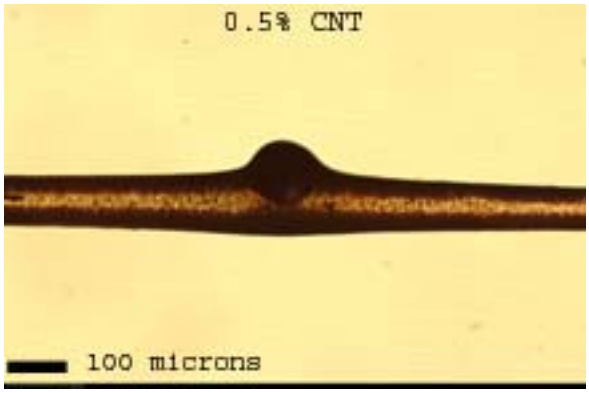

Figure 4.24

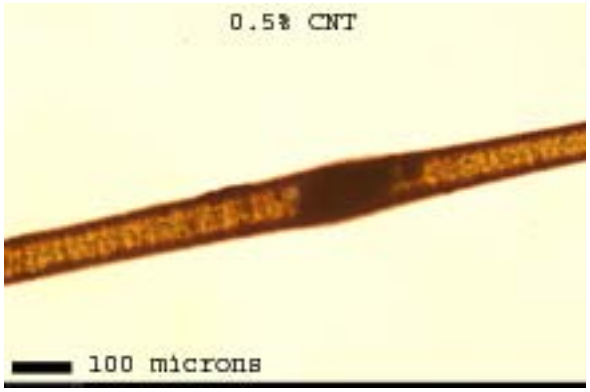

Figure 4.25

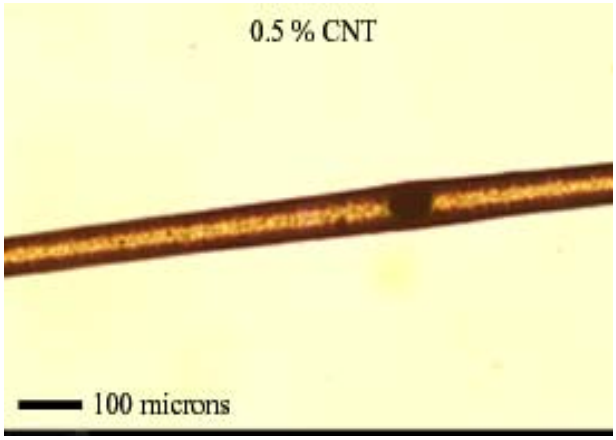

Figure 4.26

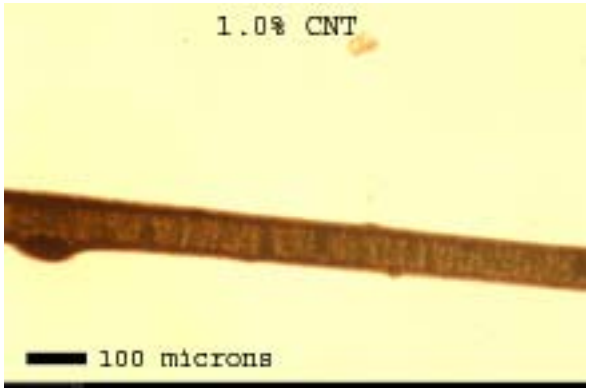

Figure 4.27

Figure 4.28

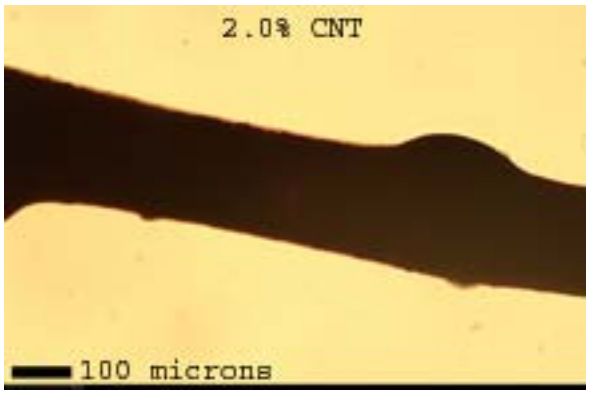

Figure 4.29

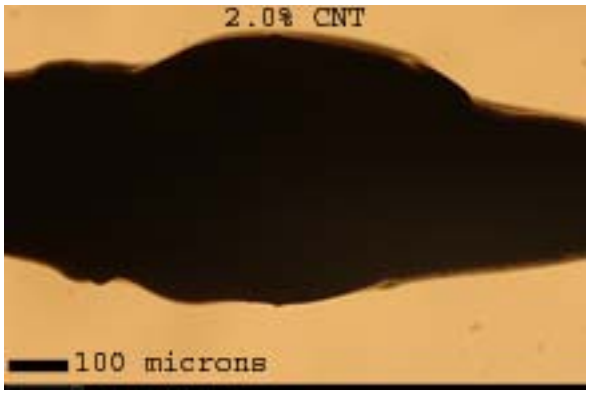

Figure 4.30

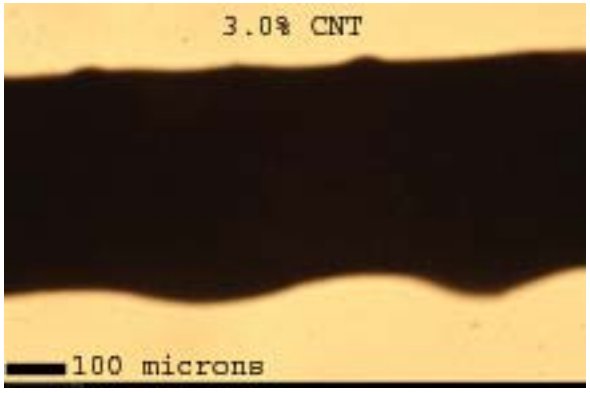

Figure 4.31

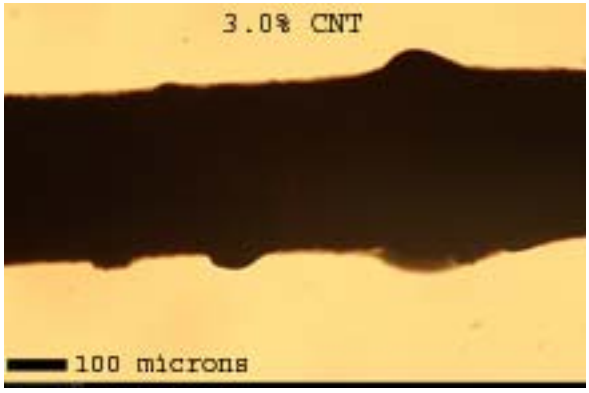

Figure 4.32

The SEM photographs also show the heavy disfiguration of the fibers by the nanotube agglomerates. The disfiguration is more sever at the 2.0% and 3.0% loading, figure 4.38-4.41.

Scanning Electron Microscopy

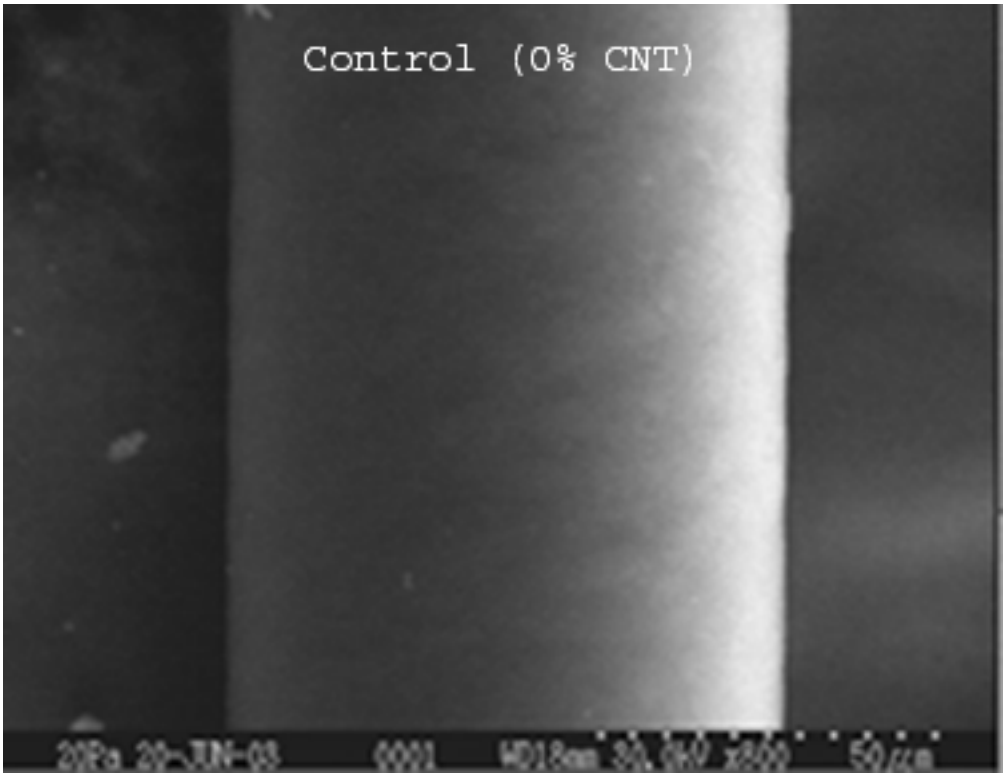

Figure 4.33

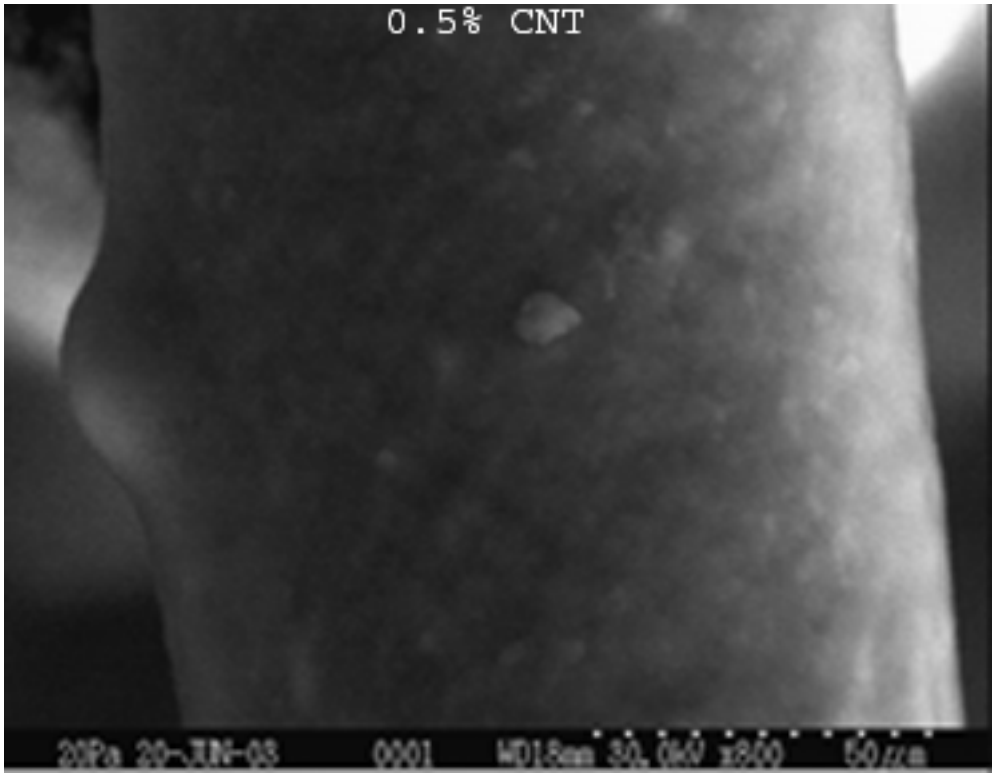

Figure 4.34

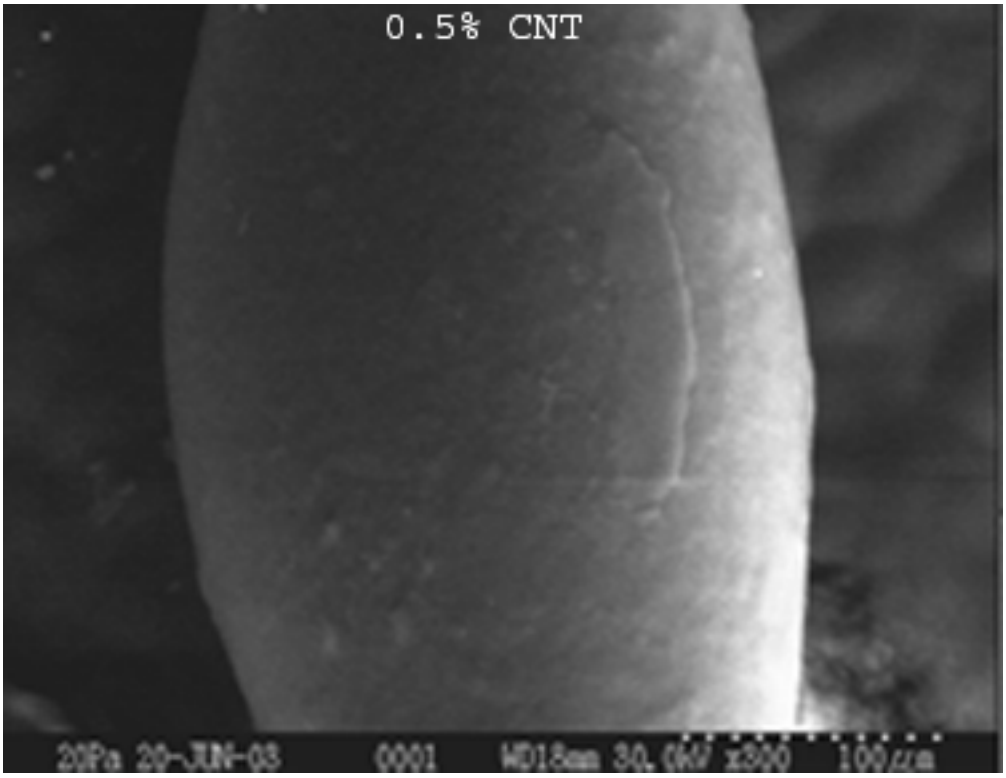

Figure 4.35

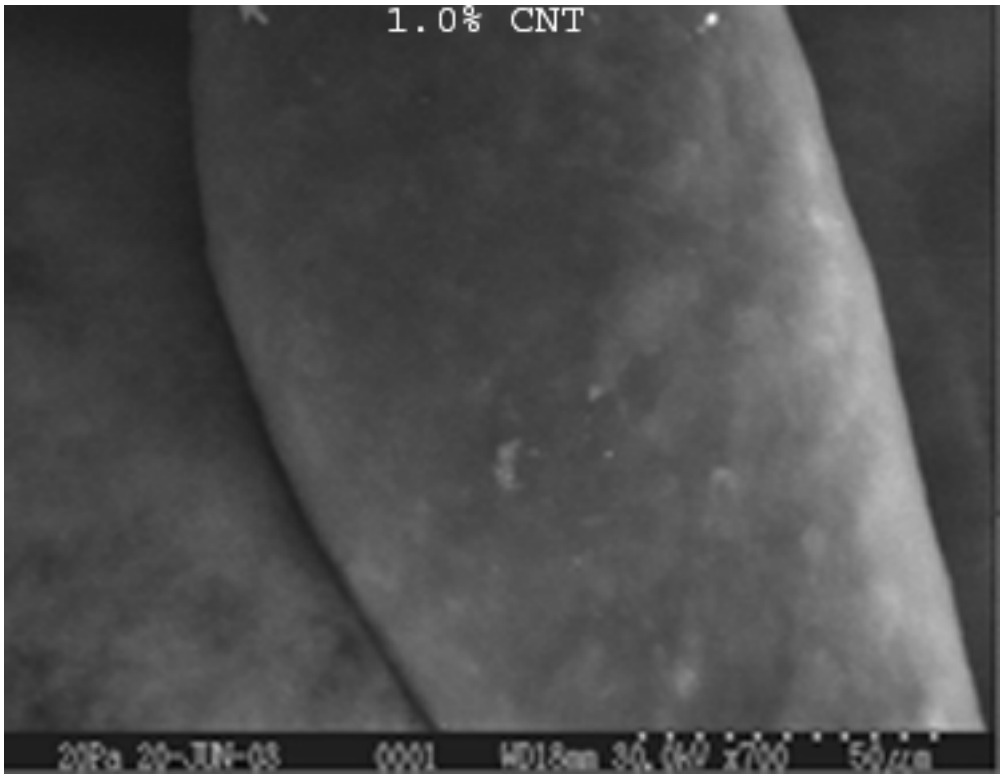

Figure 4.36

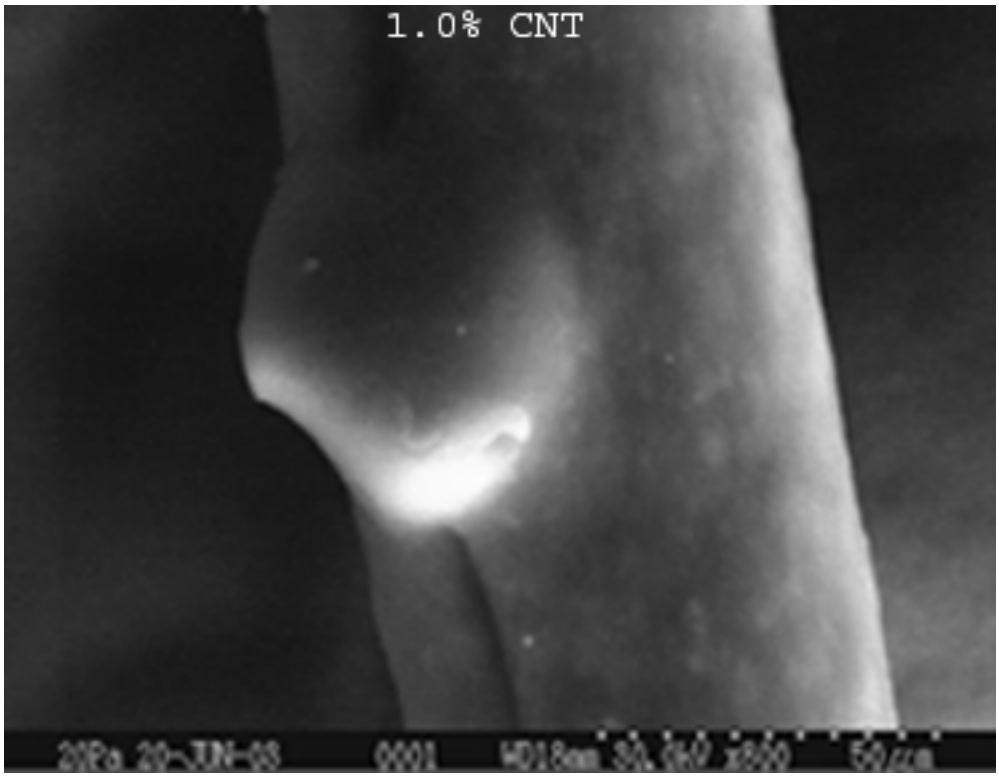

Figure 4.37

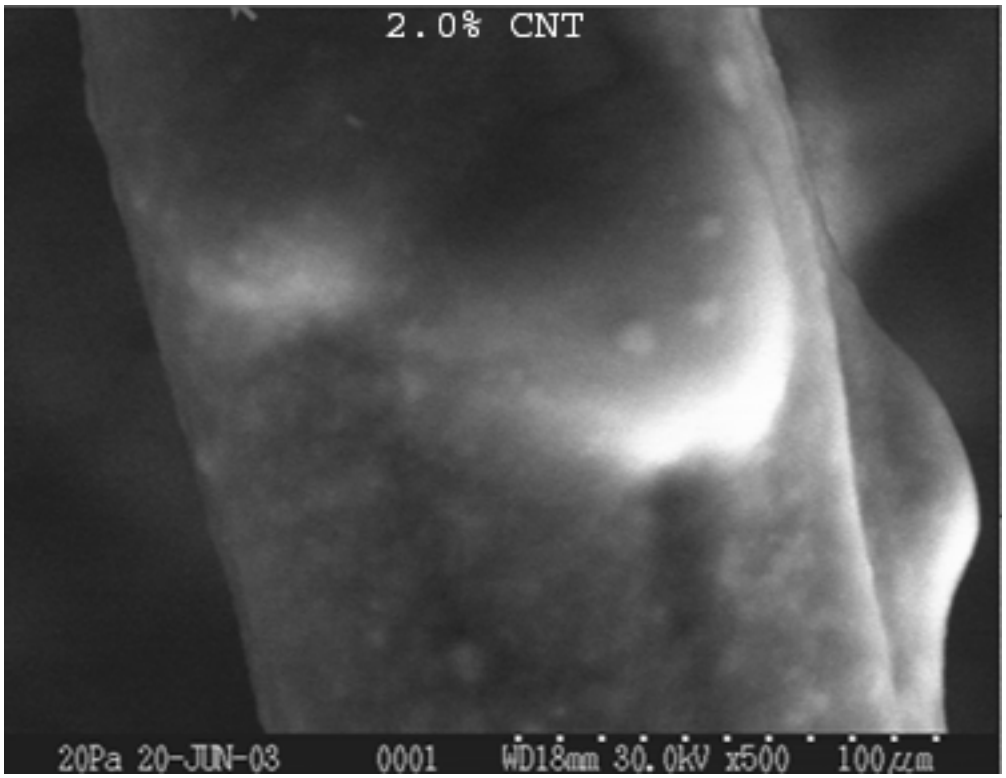

Figure 4.38

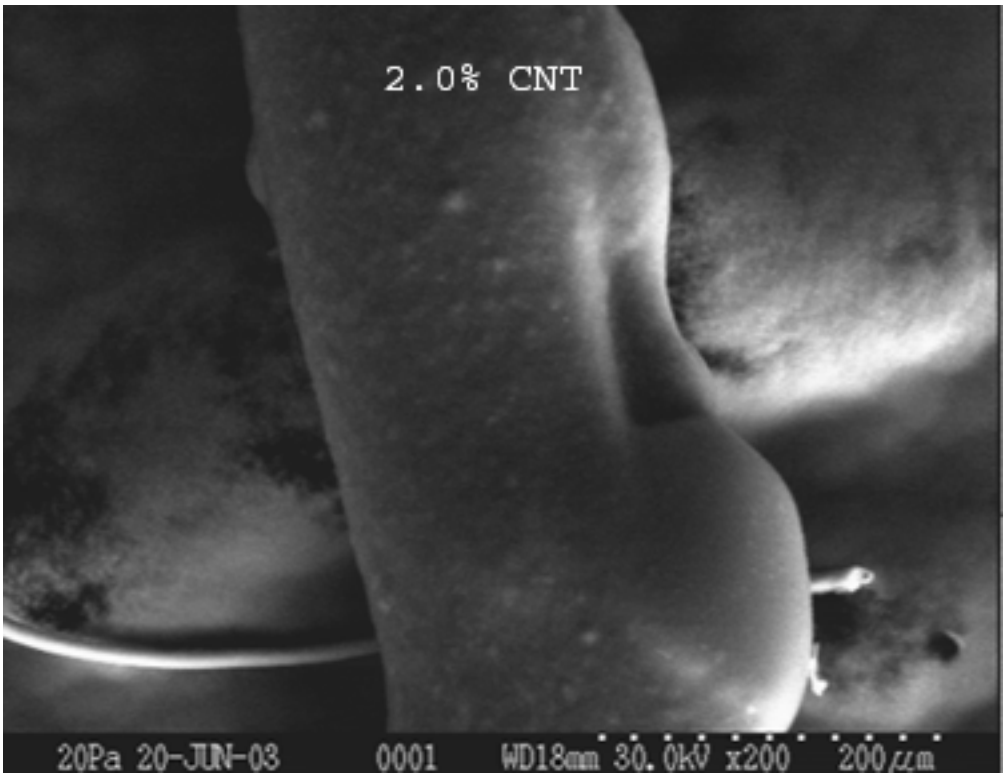

Figure 4.39

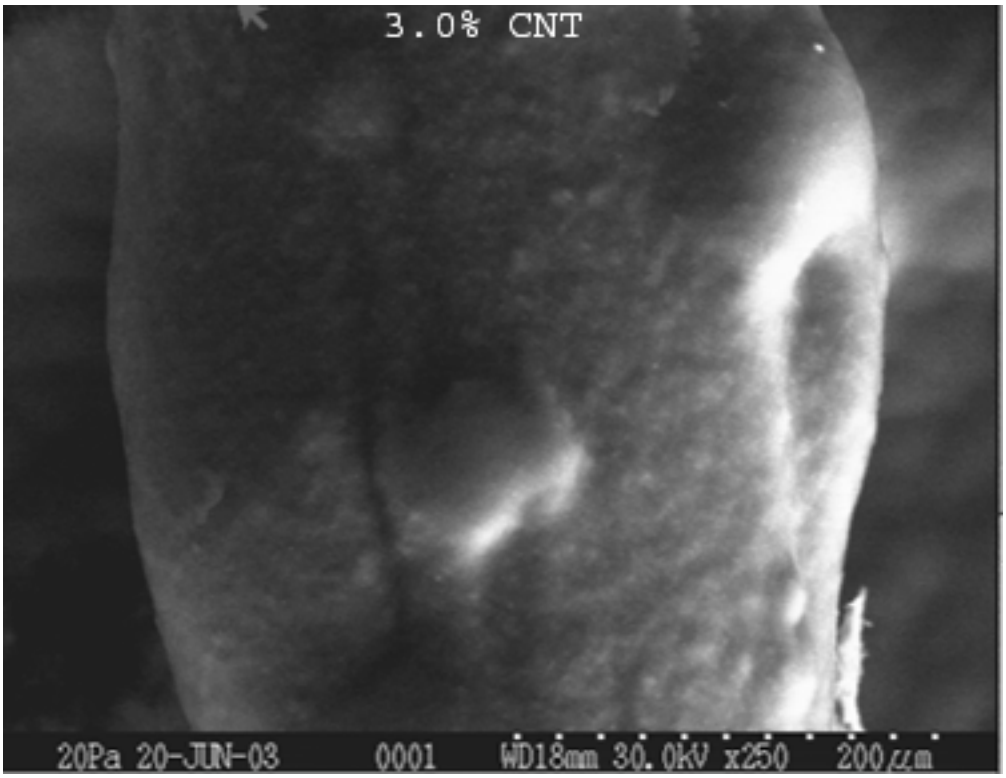

Figure 4.40

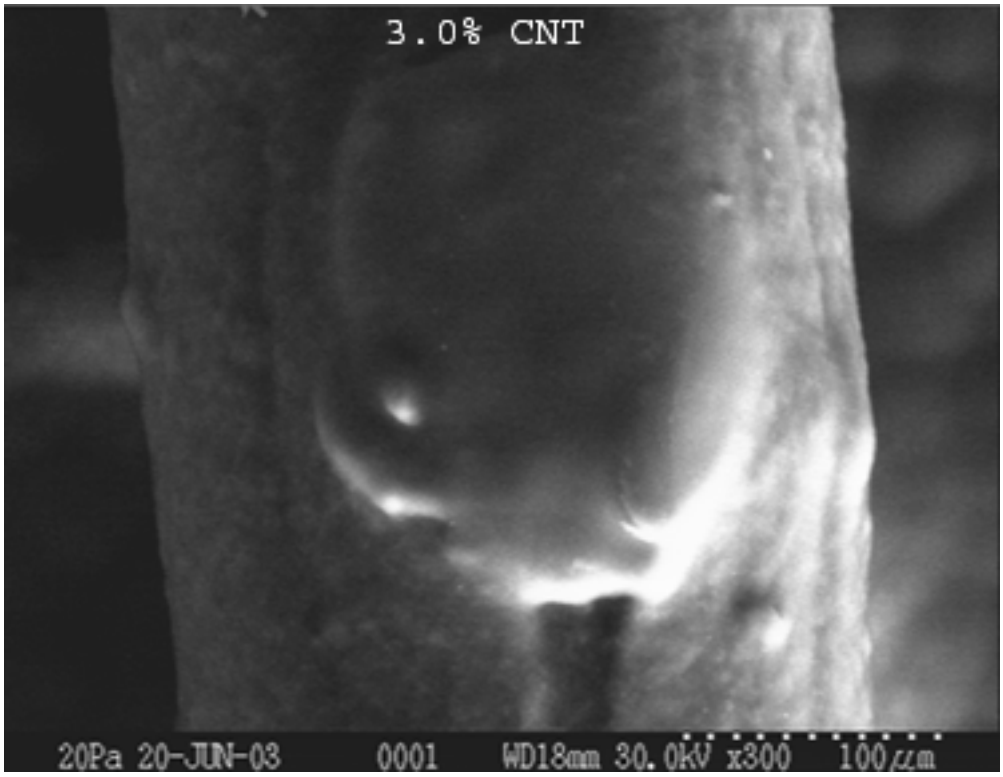

Figure 4.41

Conductivity

All fibers had a resistance of greater than 1 mega ohm per inch and are not conductive. Good dispersion is critical for percolation at low load levels. CNT aggregation inhibits the formation of a continuous network within the fibers by concentrating the nanotubes in certain areas.

Chapter Five

Conclusions

The distribution of the CNT in the polypropylene is critical to spinning uniform fibers. Visual inspection and worsened mechanical properties prove that twin screw compounding followed by single screw extrusion creates a non-uniform distribution of CNTs throughout the fiber. The CNT aggregation prevents percolation and the formation of a conductive fiber, as evidenced through the conductivity test. The CNT aggregation prevents the CNT from acting as reinforcement and causes premature fiber breakage due to stress concentrations. The CNT aggregation prevents fiber drawing. CNT aggregation remains a challenge to the processing of these composite fibers.

Chapter Six

Recommendations for Future Work

The issue of poor dispersion needs to be addressed in detail. Without first conquering this problem, the possible advantages of improved mechanical properties and conduction are moot points.

Start with carbon nanotubes that are single walled and not multi-walled. The single walled nanotubes have more uniform characteristics and thus give more uniform characteristics to resultant fibers.

Spinning conditions need to be consistent throughout the experiment so that the effect of CNT load alone on fiber properties only may be address. Experiments should be run to determine what the optimum processing conditions are.

References

[1] Ku, Chen C. and Raimond Liepins. Electrical Properties of Polymers: Chemical Principles. New York: Macmillan Publishing Company, 1987

[2] Karger-Kocsis J., ed. Polypropylene: an A – Z Reference. Dordrecht: Kluwer Academic Publishers, 1999.

[3] Seanor, Donald A, ed. Electrical Properties of Polymers. New York: Academic Press Inc, 1982.

[4] Murphy, John. Additives for Plastics Handbook, 2nd ed. Oxford: Elsevier Advanced Technology, 2001.

[5] Wirsen, Anders. Electroactive Polymer Materials: State of the Art Review of Conductive Polymers. Lancaster, PA: Technomic Publishing Company, 1986.

[6] Kumar, Satish et al. " Fibers from polypropylene/nano carbon fiber composites." Polymer **43** (2002) 1701-1703.

[7] Seymour, Richard, ed. Conductive Polymers. New York: Plenum Press, 1981.

[8] Skotheim, TerjeA., Ronald Elsenbaumer and John Renolds, ed. Handbook of Conducting Polymers. New York: Marcell Dekker, Inc, 1998.

[9] Kothari, V.K, ed. Textile Fibers: Development and Innovations. New Delhi: IAFL Publications, 2000.

[10] Stauffer, D. and A. Aharony. " Percolation." Encyclopedia of Physical Science and Technology. Third Ed. Volume 11, Academic Press, 2002.

[11] Roldughin, V.I. and V.V. Vystoskii. "Review: Percolation Properties of metal-filled polymer films, structure and mechanisms of conductivity." Progression in Organic Coatings **39**, 81-100 (2002).

[12] Thongruang,Wiriya, Richard J. Spontak and C. Maurice Balik. "Correlated electrical conductivity and mechanical property analysis of high-density polyethylene filled with graphite and carbon fiber." Polymer **43**, 3717-3725 (2002).

[13] Thostenson, Erik T., Zhifeng Ren and Tsu-Wei Chou. Advances in the science and technology of carbon nanotubes and their composites: a review, *Composite Science and Technology*, **61**, 1899-1912 (2001).

[14] Lau, Alan Kin Tak and David Hui. The revolutionary creation of new advanced materials-carbon nanotube composites, *Composites: Part B,* **33**, 263-267 (2002).

[15] Salvetat-Delmotee, Jean-Paul and Angel Rubio. Mechanical Properties of carbon nanotubes: a fiber digest for beginners, *Carbon*, **40**, 1729-1734 (2002).

[16] Method for forming a fibers/composite material having an anisotropic structure, **U.S. Patent No. 6,299,812 B1** October 9, 2001.

[17] Cooper, Carole, Diana Ravich, David Lips, Joerg Mayer and H. Daniel Wagner. Distribution and alignment of carbon nanotubes and nanofibrils in a polymer matrix, *Composites Science and Technology,* **62,** 1105-112 (2002).

[18] Haggenmueller, R., H.H. Gommans, A.G.Rinzler, J.E. Fischer and K.I. Winey. Aligned single-walled carbon nanotubes in composites by melt processing methods. *Chemical Physical Letters*, **330**, 219-225 (2000).

[19] Godeyev, S.A. et al. "A promising conductive material: highly orientated Polypropylene filled with short vapor-grown carbon fibers" Material Letters **51** 32-36 (2001).

[20] Gupta, V.B. and V.K. Kothari, ed. Manufactured Fibre Technology. London: Chapman & Hall, 1997.

Appendix I

Spinning Conditions

Trial I

Spinning Conditions for Trial I

Polymer used	PP 1[1] - 100%	PP 1 - 100%	PP 1 - 100%	PP 1 - 100%	PP 1 - 100%	PP 1 - 100%	PP 1 - 100%	PP 1 - 100%	PP 1 - 100%
Spinneret Information									
Pack formula	A[2]	A	A	A	A	A	A	A	A
Both pump rpm	13.27	13.27	13.27	13.27	13.27	13.27	13.27	13.45	13.45
Spin Head Temperature, °C	204	204	204	226	226	227	240	240	244
Hole Type	round mono-filament	round mono-filament	round mono-filament	round mono-filament	round mono-filament	round mono-filament	round mono-filament	round mono-filament	round mono-filament
Number of Holes	72	72	72	72	72	72	72	72	72
Hole Diameter, mm	0.6	0.6	0.6	0.6	0.6	0.6	0.6	0.6	0.6
Avg. Melt Pump Pressure AA BB	852	861	867	710	705	699	624	635	638
Roller Speed (m/min)									
Denier Roll	792	992	1192	792	992	1192	792	992	1192
Feed Roll	794	994	1194	794	994	1194	794	994	1194
Draw 1 Roll	797	997	1197	797	997	1197	797	997	1197
Draw 2 Roll	800	1000	1200	800	1000	1200	800	1000	1200
Leesona Winder	815	1015	1215	815	1015	1215	815	1015	1215
Spun Denier (g/9000m)	14.4	11.6	9.7	14.4	11.6	9.7	14	11.4	9.6
Comments	Spun ok	Spun ok	Spun ok	Spun ok	Spun ok	Spun ok	Spun ok	Spun ok	Spun ok

[1] PP 1 designates the polymer as Equistar, Petrothene ™ Type PP51B30V LotBPP2121506 MFR 30

[2] A designates the pack formula as consisting of 4 screens: 20,80,180, and 325 mesh

Spin Conditions for Trail I (continued)

Polymer used				
	PP 1 - 100%	PP 1 - 100%	PP 1 - 100%	PP 1- 99.5% / Nano 1[4]- 0.5%
Spinneret Information				
Pack formula	B[3]	B	B	A
Both pump rpm	13.85	13.85	13.85	13.85
Spin Head Temperature, °C	241	243	245	240
Hole Type	round mono-filament	round mono-filament	round mono-filament	round mono-filament
Number of Holes	72	72	72	72
Hole Diameter, mm	1.1	1.1	1.1	1.1
Avg. Melt Pump Pressure AA				Start Pressure: 708 psi
BB	482	479	477	Increase Rate 1,660 psi/hr4
Roller Speed (m/min)				
Denier Roll	792	992	1192	992
Feed Roll	794	994	1194	994
Draw 1 Roll	797	997	1197	997
Draw 2 Roll	800	1000	1200	1000
Leesona Winder	815	1015	1215	1015
Spun Denier (g/9000m)	14.7	11.8	9.8	11.8
Comments	Spun ok	Spun ok	Spun ok	Partial tube made. Broke after transition. Black globs observed. Conclude poor mixing and agglomeration

[3]B designates the pack formula as consisting of 2 screens: 20, and 80 mesh

[4] Nano 1 designates the polymer as Hyperion Catalysis Polyproplyene with Fibril™ nanotubes 15% concentration by weigth; Lot 309-09-01

Appendix II

Spinning Conditions

Trial II

Spinning Conditions for Trial II

Polymer used	PP3[5] 0% CNT	PP3 0.5% CNT	PP3 1.0% CNT	PP3 2. 0% CNT	PP3 3. 0% CNT
Spinneret Information					
Pack formula	C[6]	C	C	C	C
Both pump rpm	10.87	10.87	10.87	10.9	
Spin Head Temperature, ^{o}C	218	249	220	289	
Hole Type	round mono-filament	round mono-filament	round mono-filament	round mono-filament	round mono-filament
Number of Holes	44	44	44	44	44
Hole Diameter, mm	1.5	1.5	1.5	1.5	1.5
Roller Speed (m/min)					
Denier Roll	392	392	392	192	N/A
Feed Roll	393	393	393	195	N/A
Draw 1 Roll	393	396	396	199	N/A
Draw 2 Roll	400	400	400	N/A	N/A
Leesona Winder	415	415	415	220	N/A
Comments	Spun Ok				Too weak to thread up

[5] PP 3 designates the polymer as Equistar PP compounded with Hyperion Catalysis PP(with 15% CNT) at the % by weight as shown

[6] C designates the pack formula as consisting of 1 screen, 20 mesh

Spin Conditions for Trail II (continued)

Sheath / Core Ratio	60 / 40	40 / 60	20 / 80	70 / 30	50 / 50	20 / 80
Polymer used	PP3 1.0% CNT	PP3 1.0% CNT	PP3 1.0% CNT	PP3 3. 0% CNT	PP3 3. 0% CNT	PP3 3. 0% CNT
Spinneret Information						
Pack formula	C	C	C	C	C	C
Spin Head Temperature, ^{o}C	240	240	240	240	200	242
Hole Type	round mono-filament	round mono-filament	round mono-filament	round mono-filament	round mono-filament	round mono-filament
Number of Holes	44	44	44	44	44	44
Hole Diameter, mm	1.5	1.5	1.5	1.5	1.5	1.5
Roller Speed (m/min)						
Denier Roll	392		392		N/A	N/A
Feed Roll	396		395		N/A	N/A
Draw 1 Roll	397		396		N/A	N/A
Draw 2 Roll	400		400		N/A	N/A
Leesona Winder	415		415	200	N/A	N/A
Comments					Too weak to thread up	Too weak to thread up

Appendix III

Statistical Analysis

Fiber Denier

TREATMENT	N	Maximum	Minimum	Average	Standard Deviation
0%	20	42.73	17.31	30.25	7.0553
0.50%	20	94.76	25.40	41.21	17.9816
1.00%	20	134.99	34.10	51.53	23.8704
2.00%	21	282.60	45.90	115.84	62.1946
3.00%	20	321.30	121.50	199.85	49.7011

Fiber Denier

Treatment	Treatment	Estimate	StdErr	DF	tValue	Probt	Result
0%	0.50%	-10.9602	12.1712	96	-0.9005	3.70E-01	Not Significantly Different
0%	1.00%	-21.2877	12.1712	96	-1.7490	8.35E-02	Not Significantly Different
0%	2.00%	-85.5970	12.0254	96	-7.1180	1.98E-10	Significantly Different
0%	3.00%	-169.5992	12.1712	96	-13.9345	8.64E-25	Significantly Different
0.50%	1.00%	-10.3275	12.1712	96	-0.8485	3.98E-01	Not Significantly Different
0.50%	2.00%	-74.6368	12.0254	96	-6.2066	1.37E-08	Significantly Different
0.50%	3.00%	-158.6390	12.1712	96	-13.0340	5.86E-23	Significantly Different
1.00%	2.00%	-64.3093	12.0254	96	-5.3478	6.02E-07	Significantly Different
1.00%	3.00%	-148.3115	12.1712	96	-12.1854	3.37E-21	Significantly Different
2.00%	3.00%	-84.0021	12.0254	96	-6.9854	3.72E-10	Significantly Different

Bicomponent Fiber Denier (1% Core)

TREATMENT	N	Maximum	Minimum	Average	Standard Deviation
100/0 1%	20	134.991	34.101	51.53355	23.87039089
20/80 1%	20	118.548	11.358	37.485	28.27474448
40/60 1%	20	70.488	11.826	37.35765	14.03272958
60/40 1%	20	56.601	11.106	30.99825	14.85721945

Bicomponent Fiber Denier (1% Core)

Treatment	Treatment	Estimate	StdErr	DF	tValue	Probt	Result
100/0 1%	20/80 1%	14.04855	6.6838	76	2.10189	0.038876	Significantly Different
100/0 1%	40/60 1%	14.1759	6.6838	76	2.120944	0.037188	Significantly Different
100/0 1%	60/40 1%	20.5353	6.6838	76	3.072413	0.002947	Significantly Different
20/80 1%	40/60 1%	0.12735	6.6838	76	0.019054	0.984848	Not Significantly Different
20/80 1%	60/40 1%	6.48675	6.6838	76	0.970523	0.334865	Not Significantly Different
40/60 1%	60/40 1%	6.3594	6.6838	76	0.951469	0.344383	Not Significantly Different

Bicomponent Fiber Denier (3% Core)

TREATMENT	N	Maximum	Minimum	Average	Standard Deviation
100/0 3%	20	321.30	121.50	199.85	49.7011
30/70 3%	20	62.29	8.32	21.94	14.8412
50/50 3%	20	52.14	9.44	31.94	11.9182
20/80 3%	20	262.80	90.90	168.53	62.8088

Bicomponent Fiber Denier (3% Core)

Treatment	Treatment	Estimate	StdErr	DF	tValue	Probt	Result
100/0 3%	30/70 3%	177.90075	13.01676624	76	13.66704654	3.6132E-22	Significantly Different
100/0 3%	50/50 3%	167.9076	13.01676624	76	12.89933282	7.91512E-21	Significantly Different
100/0 3%	20/80 3%	31.32	13.01676624	76	2.406127561	0.018552919	Significantly Different
30/70 3%	50/50 3%	-9.99315	13.01676624	76	-0.767713717	0.445035989	Not Significantly Different
30/70 3%	20/80 3%	-146.58075	13.01676624	76	-11.26091898	7.25197E-18	Significantly Different
50/50 3%	20/80 3%	-136.5876	13.01676624	76	-10.49320526	1.95082E-16	Significantly Different

Fiber Breaking Stress

TREATMENT	N	Maximum	Minimum	Average	Standard Deviation
0%	20	2.8521	1.4886	2.1128	0.3426
0.50%	20	1.0618	0.4709	0.6875	0.1198
1.00%	21	1.3379	0.4970	0.7016	0.1758
2.00%	22	0.3958	0.1497	0.2482	0.0676
3.00%	21	1.6976	0.6678	1.1090	0.3232
60/40 1.00%	24	1.3877	0.0492	0.8221	0.2634
40/60 1.00%	23	1.2274	0.4941	0.8119	0.2016
20/80 1.00%	24	1.0751	0.0309	0.5902	0.2497
70/30 3.00%	21	2.3022	0.2673	1.0470	0.5945
50/50 3.00%	21	1.3781	0.4920	0.7997	0.2572
20/80 3.00%	22	0.2399	0.0910	0.1417	0.0381

Fiber Breaking Stress

Treatment	Treatment	Estimate	StdErr	DF	tValue	Probt	Result
0%	**0.50%**	1.4253	0.0880	228	16.1947	8.949E-40	Significantly Different
0%	**1.00%**	1.4111	0.0870	228	16.2280	6.95692E-40	Significantly Different
0%	**2.00%**	1.8646	0.0860	228	21.6842	2.49944E-57	Significantly Different
0%	**3.00%**	1.0038	0.0870	228	11.5433	1.41503E-24	Significantly Different
0%	**60/40 1.00%**	1.2907	0.0843	228	15.3172	6.87551E-37	Significantly Different
0%	**40/60 1.00%**	1.3009	0.0851	228	15.2880	8.5827E-37	Significantly Different
0%	**20/80 1.00%**	1.5226	0.0843	228	18.0694	6.8503E-46	Significantly Different
0%	**70/30 3.00%**	1.0658	0.0870	228	12.2569	7.248E-27	Significantly Different
0%	**50/50 3.00%**	1.3131	0.0870	228	15.1006	3.5527E-36	Significantly Different
0%	**20/80 3.00%**	1.9655	0.0860	228	22.8575	6.56306E-61	Significantly Different
0.50%	**1.00%**	-0.0142	0.0870	228	-0.1630	0.870666786	Not Significantly Different
0.50%	**2.00%**	0.4393	0.0860	228	5.1084	6.86049E-07	Significantly Different
0.50%	**3.00%**	-0.4215	0.0870	228	-4.8478	2.31003E-06	Significantly Different
0.50%	**60/40 1.00%**	-0.1346	0.0843	228	-1.5976	0.111520977	Not Significantly Different
0.50%	**20/80 1.00%**	0.0973	0.0843	228	1.1546	0.249476066	Not Significantly Different
0.50%	**70/30 3.00%**	-0.3595	0.0870	228	-4.1341	5.00951E-05	Significantly Different
1.00%	**2.00%**	0.4534	0.0849	228	5.3403	2.24152E-07	Significantly Different
1.00%	**3.00%**	-0.4074	0.0859	228	-4.7430	3.71372E-06	Significantly Different
1.00%	**60/40 1.00%**	-0.1204	0.0832	228	-1.4483	0.14890379	Not Significantly Different
1.00%	**20/80 1.00%**	0.1115	0.0832	228	1.3403	0.181484271	Not Significantly Different
1.00%	**70/30 3.00%**	-0.3453	0.0859	228	-4.0204	7.89818E-05	Significantly Different
2.00%	**3.00%**	-0.8608	0.0849	228	-10.1381	3.54207E-20	Significantly Different
2.00%	**20/80 1.00%**	-0.3420	0.0821	228	-4.1629	4.45723E-05	Significantly Different
2.00%	**70/30 3.00%**	-0.7987	0.0849	228	-9.4072	5.7179E-18	Significantly Different
3.00%	**20/80 1.00%**	0.5188	0.0832	228	6.2388	2.12227E-09	Significantly Different

Fiber Breaking Stress (continued)

Treatment	Treatment	Estimate	StdErr	DF	tValue	Probt	Result
60/40 1.00%	**2.00%**	0.5739	0.0821	228	6.9859	3.07686E-11	Significantly Different
60/40 1.00%	**3.00%**	-0.2869	0.0832	228	-3.4502	0.000667307	Significantly Different
60/40 1.00%	**20/80 1.00%**	0.2319	0.0803	228	2.8865	0.004270017	Significantly Different
60/40 1.00%	**70/30 3.00%**	-0.2249	0.0832	228	-2.7040	0.007368423	Significantly Different
40/60 1.00%	**0.50%**	0.1244	0.0851	228	1.4621	0.145081896	Not Significantly Different
40/60 1.00%	**1.00%**	0.1102	0.0840	228	1.3124	0.190708884	Not Significantly Different
40/60 1.00%	**2.00%**	0.5637	0.0830	228	6.7915	9.5338E-11	Significantly Different
40/60 1.00%	**3.00%**	-0.2971	0.0840	228	-3.5372	0.000489896	Significantly Different
40/60 1.00%	**60/40 1.00%**	-0.0102	0.0812	228	-0.1256	0.900140507	Not Significantly Different
40/60 1.00%	**20/80 1.00%**	0.2217	0.0812	228	2.7300	0.006828366	Significantly Different
40/60 1.00%	**70/30 3.00%**	-0.2351	0.0840	228	-2.7984	0.005575344	Significantly Different
70/30 3.00%	**3.00%**	-0.0621	0.0859	228	-0.7225	0.470705433	Not Significantly Different
70/30 3.00%	**20/80 1.00%**	0.4568	0.0832	228	5.4926	1.05454E-07	Significantly Different
50/50 3.00%	**0.50%**	0.1122	0.0870	228	1.2904	0.198221028	Not Significantly Different
50/50 3.00%	**1.00%**	0.0980	0.0859	228	1.1414	0.254899051	Not Significantly Different
50/50 3.00%	**2.00%**	0.5515	0.0849	228	6.4949	5.14705E-10	Significantly Different
50/50 3.00%	**3.00%**	-0.3093	0.0859	228	-3.6015	0.00038821	Significantly Different
50/50 3.00%	**60/40 1.00%**	-0.0224	0.0832	228	-0.2695	0.787808748	Not Significantly Different
50/50 3.00%	**40/60 1.00%**	-0.0122	0.0840	228	-0.1453	0.884578074	Not Significantly Different
50/50 3.00%	**20/80 1.00%**	0.2095	0.0832	228	2.5191	0.012450038	Significantly Different
50/50 3.00%	**70/30 3.00%**	-0.2473	0.0859	228	-2.8790	0.004368719	Significantly Different
20/80 3.00%	**0.50%**	-0.5401	0.0860	228	-6.2817	1.67817E-09	Significantly Different
20/80 3.00%	**1.00%**	-0.5543	0.0849	228	-6.5285	4.26238E-10	Significantly Different
20/80 3.00%	**2.00%**	-0.1009	0.0839	228	-1.2023	0.230510559	Significantly Different
20/80 3.00%	**3.00%**	-0.9617	0.0849	228	-11.3263	6.93063E-24	Significantly Different
20/80 3.00%	**60/40 1.00%**	-0.6748	0.0821	228	-8.2140	1.59624E-14	Significantly Different
20/80 3.00%	**40/60 1.00%**	-0.6646	0.0830	228	-8.0070	5.98787E-14	Significantly Different
20/80 3.00%	**20/80 1.00%**	-0.4429	0.0821	228	-5.3910	1.74685E-07	Significantly Different
20/80 3.00%	**70/30 3.00%**	-0.8996	0.0849	228	-10.5954	1.37208E-21	Significantly Different
20/80 3.00%	**50/50 3.00%**	-0.6524	0.0849	228	-7.6831	4.56913E-13	Significantly Different

Fiber Breaking Strain

TREATMENT	N	Maximum	Minimum	Average	Standard Deviation
0%	20	1009.46	524.56	845.27	138.02
0.50%	20	786.42	347.95	502.52	101.14
1.00%	21	675.95	251.23	472.20	98.32
2.00%	22	465.96	113.34	264.43	97.79
3.00%	21	203.42	2.70	46.84	66.61
60/40 1.00%	24	866.70	1.32	494.57	193.75
40/60 1.00%	23	927.88	346.82	699.85	132.06
20/80 1.00%	24	676.92	1.93	480.38	135.75
70/30 3.00%	21	682.92	147.59	495.20	137.70
50/50 3.00%	21	884.86	419.10	686.35	131.86
20/80 3.00%	22	680.47	310.81	502.91	114.95

Fiber Breaking Strain

Treatment	Treatment	Estimate	StdErr	DF	tValue	Probt	Result
0%	**0.50%**	342.7502	38.9298	227	8.8043	3.42266E-16	Significantly Different
0%	**1.00%**	373.0776	38.4636	227	9.6995	7.83086E-19	Significantly Different
0%	**2.00%**	580.8446	38.0347	227	15.2714	1.07641E-36	Significantly Different
0%	**3.00%**	798.4308	38.4636	227	20.7581	2.30252E-54	Significantly Different
0%	**60/40 1.00%**	329.5209	37.6390	227	8.7548	4.7546E-16	Significantly Different
0%	**40/60 1.00%**	145.4233	37.6390	227	3.8636	0.000145796	Significantly Different
0%	**20/80 1.00%**	364.8881	37.2724	227	9.7898	4.18572E-19	Significantly Different
0%	**70/30 3.00%**	350.0758	38.4636	227	9.1015	4.67881E-17	Significantly Different
0%	**50/50 3.00%**	158.9208	38.4636	227	4.1317	5.06477E-05	Significantly Different
0%	**20/80 3.00%**	350.1907	38.0347	227	9.2071	2.29013E-17	Significantly Different
0.50%	**1.00%**	30.3273	38.4636	227	0.7885	0.431245241	Not Significantly Different
0.50%	**2.00%**	238.0943	38.0347	227	6.2599	1.90289E-09	Significantly Different
0.50%	**3.00%**	455.6806	38.4636	227	11.8471	1.58964E-25	Significantly Different
0.50%	**60/40 1.00%**	-13.2293	37.6390	227	-0.3515	0.725555018	Not Significantly Different
0.50%	**20/80 1.00%**	22.1379	37.2724	227	0.5939	0.553138981	Not Significantly Different
0.50%	**70/30 3.00%**	7.3255	38.4636	227	0.1905	0.849123517	Not Significantly Different
1.00%	**2.00%**	207.7670	37.5574	227	5.5320	8.68934E-08	Significantly Different
1.00%	**3.00%**	425.3532	37.9916	227	11.1960	1.87007E-23	Significantly Different
1.00%	**60/40 1.00%**	-43.5566	37.1565	227	-1.1722	0.242326654	Not Significantly Different
1.00%	**20/80 1.00%**	-8.1895	36.7852	227	-0.2226	0.824024432	Not Significantly Different
1.00%	**70/30 3.00%**	-23.0018	37.9916	227	-0.6054	0.545489095	Not Significantly Different
2.00%	**3.00%**	217.5862	37.5574	227	5.7934	2.28636E-08	Significantly Different
2.00%	**70/30 3.00%**	-230.7688	37.5574	227	-6.1444	3.5641E-09	Significantly Different
2.00%	**20/80 1.00%**	-215.9565	36.3366	227	-5.9432	1.0438E-08	Significantly Different
3.00%	**20/80 1.00%**	-433.5427	36.7852	227	-11.7858	2.49677E-25	Significantly Different

Fiber Breaking Strain (continued)

Treatment	Treatment	Estimate	StdErr	DF	tValue	Probt	Result
60/40 1.00%	**2.00%**	251.3236	36.7124	227	6.8457	7.02667E-11	Significantly Different
60/40 1.00%	**3.00%**	468.9099	37.1565	227	12.6199	5.14235E-28	Significantly Different
60/40 1.00%	**20/80 1.00%**	35.3672	35.9221	227	0.9846	0.325892441	Not Significantly Different
60/40 1.00%	**70/30 3.00%**	20.5548	37.1565	227	0.5532	0.580673424	Not Significantly Different
40/60 1.00%	**0.50%**	197.3270	37.6390	227	5.2426	3.61843E-07	Significantly Different
40/60 1.00%	**1.00%**	227.6543	37.1565	227	6.1269	3.91763E-09	Significantly Different
40/60 1.00%	**2.00%**	435.4213	36.7124	227	11.8603	1.4417E-25	Significantly Different
40/60 1.00%	**3.00%**	653.0075	37.1565	227	17.5745	3.18427E-44	Significantly Different
40/60 1.00%	**60/40 1.00%**	184.0977	36.3022	227	5.0712	8.2051E-07	Significantly Different
40/60 1.00%	**20/80 1.00%**	219.4648	35.9221	227	6.1095	4.30321E-09	Significantly Different
40/60 1.00%	**70/30 3.00%**	204.6525	37.1565	227	5.5078	9.80776E-08	Significantly Different
70/30 3.00%	**3.00%**	448.3550	37.9916	227	11.8014	2.22521E-25	Significantly Different
70/30 3.00%	**20/80 1.00%**	14.8123	36.7852	227	0.4027	0.68756961	Not Significantly Different
50/50 3.00%	**0.50%**	183.8294	38.4636	227	4.7793	3.16009E-06	Significantly Different
50/50 3.00%	**1.00%**	214.1567	37.9916	227	5.6370	5.11029E-08	Significantly Different
50/50 3.00%	**2.00%**	421.9238	37.5574	227	11.2341	1.41725E-23	Significantly Different
50/50 3.00%	**3.00%**	639.5100	37.9916	227	16.8329	8.23857E-42	Significantly Different
50/50 3.00%	**60/40 1.00%**	170.6001	37.1565	227	4.5914	7.29353E-06	Significantly Different
50/50 3.00%	**40/60 1.00%**	-13.4975	37.1565	227	-0.3633	0.716747699	Not Significantly Different
50/50 3.00%	**20/80 1.00%**	205.9673	36.7852	227	5.5992	6.19065E-08	Significantly Different
50/50 3.00%	**70/30 3.00%**	191.1550	37.9916	227	5.0315	9.89253E-07	Significantly Different
20/80 3.00%	**0.50%**	-7.4404	38.0347	227	-0.1956	0.845081137	Not Significantly Different
20/80 3.00%	**1.00%**	22.8869	37.5574	227	0.6094	0.542879177	Not Significantly Different
20/80 3.00%	**2.00%**	230.6539	37.1181	227	6.2141	2.44372E-09	Significantly Different
20/80 3.00%	**3.00%**	448.2401	37.5574	227	11.9348	8.32138E-26	Significantly Different
20/80 3.00%	**60/40 1.00%**	-20.6697	36.7124	227	-0.5630	0.573978877	Not Significantly Different
20/80 3.00%	**40/60 1.00%**	-204.7674	36.7124	227	-5.5776	6.90511E-08	Significantly Different
20/80 3.00%	**20/80 1.00%**	14.6974	36.3366	227	0.4045	0.686240478	Not Significantly Different
20/80 3.00%	**70/30 3.00%**	-0.1149	37.5574	227	-0.0031	0.99756203	Not Significantly Different
20/80 3.00%	**50/50 3.00%**	-191.2699	37.5574	227	-5.0927	7.41273E-07	Significantly Different